6. FORMULATION DEVELOPMENT AND CHARACTERIZATION OF MSNs

PART A: FORMULATION OF BLANK MSNs

6.1 Introduction

Among various nanocarriers, mesoporous silica nanoparticles (MSNs) have excelled as delivery vectors owing to their large surface area, tunable pore size and release characteristics, high drug-loading capacity, zero premature release and multifunctional capability (1). MSNs also provide facile functionalization properties to design targeted systems for providing site-specific delivery and a stimuli-responsive release profile. Also, MSNs help in overcoming drug resistance with mechanisms such as endosomal delivery or co-delivery of knocking down genes with drugs and opening new avenues in the therapeutic paradigm (2). Considering their potential in constructing multifunctional composites in a single nano system, their application has further extended to development of theranostic systems. The methods for preparation of MSNs include Stober process and modified Stober process (3). The viability of all the methods described in Chapter 2 was tested and the best approach appropriate for Fulvestrant loaded Mesoporous Silica Nanoparticles (MSNs) with favourable features was further optimized.

6.2 Synthesis of Mesoporous Silica Nanoparticles

6.2.1 Synthesis of MCM – 41 types of MSNs

MCM-41 type of MSNs were synthesized using previously described procedure with little modification as described:

Typically, 1.25 gm of CTAB was dissolved in 40 ml of Distilled water at 60°C under constant stirring at 800-1000 rpm for 0.5 hours. Then 4 mL of Sodium Silicate and Triethanolamine (TEA) heated at same temperature were added dropwise into the solution under continuous stirring for another 2 hours at 60°C. The dispersion was centrifuged for 15 minutes at 12000 rpm and was filtered using vacuum filtration to recover the solid (4). The solid product was rinsed twice with methanol. The collected solid product was dried overnight at 80°C. Surfactant removal was done by the chemical reaction method (5).

6.2.1.1 Chemical reaction method for surfactant removal

To 1 gm mesoporous silica nanoparticles, 60 ml of methanol and 6 ml of 37% HCl were added in a beaker and sealed with parafilm. This dispersion was stirred on magnetic stirrer at 600 rpm for 36 hours. Afterwards, the dispersion was filtered out using vacuum filtration. The residue

was washed twice with methanol and dried at 80ºC. White feathery Mesoporous Silica Nanoparticles were obtained (6).

6.2.2 Preparation of SBA – 16 types of MSNs

SBA-16 type of MSNs were synthesized under acidic condition using sodium silicate as a silica precursor. 1 g of a structure directing agent, poloxamer 407, was dissolved in a mixture of 144 ml deionized water with 13.9 ml concentrated HCl with stirring for 30 minutes. Selected co-solvent was added in specified quantity and then required quantity of Na2SiO3 was added under stirring and the stirring was continued for another 24 h followed by aging at 100 °C temperature for 24 h in an oven. The resulting white solid was separated by filtration and washed several times with deionized water and methanol and then dried at room temperature. The collected solid product was dried overnight at 80°C. Surfactant removal was done by the chemical reaction method described in section 6.2.1.1.

Two different type of mesoporous silica nanoparticles have been synthesized: MCM-41 and SBA-16. The major difference in the synthesis of both type of nanoparticles is shown in table 6.1.

Table 6.1 Comparison of synthesis of MCM – 41 and SBA – 16 types of MSNs

Sr. No.	Parameters	MCM – 41	SBA – 15
1	pH condition	Alkaline	Acidic
2	Template/Surfactant	CTAB	Pluronic F127
3	pH regulator	Ethyl Acetate or Triethylamine (TEA)	Concentrated HCl
4	Co – Surfactant	Ethanol	IPA
5	Silica Source	Sodium silicate	TEOS
Results			
1	Particle size (nm)	65.9 ± 1.48	124.6 ± 2.36
2	% Yield (%)	94.68 ± 2.51	92.67 ± 3.14
3	Surface area (m^2/g)	1186.54 ± 31.29	741.18 ± 18.94
4	Pore size (nm)	14.21 ± 0.68	4.76 ± 0.31
5	Pore volume (cm^3/g)	3.98 ± 0.29	1.02 ± 0.13

The synthesized MSNs of both the types had significant yield of more than 80% but other parameters were superior in case of MCM – 41 types of MSN than that of SBA – 16 types. The results are shown in table 6.1. The structure of SBA types of MSN are reported to have cubic arrangement, that provides lesser surface area and the pore size was also lower due to close packing of the structure, whereas in case of MCM types of MSN, it had the hexagonal type of arrangement that had larger pore size and higher surface area due to circular shape made by array of hexagonal structure. Therefore, further optimization was carried out for MMC – 41 types of MSN.

6.2.3 Selection of Surfactant template

The surfactant screening was done by utilising different surfactants namely CTAB, CTAC, Pluronic F12 and Pluronic F68 at a concentration of 0.75% w/v. The volume of co surfactant ethanol was fixed at 3%, pH regulator TEA at 1% and silica source sodium silica at 4% (7).

Table 6.2 Screening of Surfactant template

Sr. No.	Surfactant	%Yield	Particle Size (nm)	Surface Area (m^2/g)
1	CTAB	94.16 ± 3.48	69.5 ± 1.08	1286.84
2	CTAC	83.62 ± 2.71	113.7 ± 2.69	865.23
3	Pluronic F127	75.86 ± 2.13	165.3 ± 3.96	751.38
4	Pluronic F68	71.56 ± 2.64	185.6 ± 5.29	778.62

From various surfactants, CTAB was selected for preparation of MSNs based on particle size and surface area. The particle size below 200 is desired for EPR effect, but particle size less than that of 100 nm is shown to permeate the tumor vasculature with ease and prevent the clearance of particles by phagocytic action (8). Higher the surface area, higher will be the pore volume and as the pore volume increases, more drug will be encapsulated (9).

6.2.4 Selection of Co – surfactant

Different co- surfactants, mainly alcohols, were screened as they bring about the size control and govern the pore volume and tunability of the MSN core. The co-surfactant is required to bring about the rapid diffusion of silica source and surfactant and reduce the interfacial tension between the phases (10). Methanol, ethanol, Iso propyl alcohol and Acetonitrile were screened

(11). Other parameters like surfactant concentration, silica source concentration, base catalyst concentration were kept constant (12).

Table 6.3 Selection of co – surfactant

Sr. No.	Co – Surfactant	%Yield	Particle Size (nm)	Surface Area (m^2/g)
1	Methanol	74.63 ± 2.19	93.4 ± 3.51	1011.65
2	Ethanol	95.37 ± 3.64	57.6 ± 2.16	1256.81
3	Iso propyl Alcohol	65.23 ± 1.74	112.5 ± 3.09	894.63
4	Acetonitrile	47.65 ± 2.19	138.9 ± 4.56	759.21

Ethanol was selected as a co-surfactant due to its ability to bring about rapid condensation and it behaves as weak acid in water so promotes the formation of MSN as they require basic environment for synthesis . Methanol having higher acidity compared to ethanol, made the solution with low basicity which led to decrease in yield of nanoparticles. The size also gets affected by the rate of condensation, and as the condensation was maximum with ethanol, it had lowest particle size, highest yield and higher was the surface area (13).

6.2.5 Selection of Silica Source

Silica source plays an important role in synthesis of Mesoporous Silica Nanoparticles. The sources were selected on the bases of silica concentration present in their core, their cost, and their toxicity level. Different silica sources screened were TEOS, TMOS, and Sodium silicate. The other synthesis factor had been kept constant (14, 15).

Table 6.4 Selection of Silica source

Sr. No.	Silica Source	%Yield	Particle Size (nm)	Surface Area (m^2/g)	Observation
1	TEOS	89.32 ± 4.12	86.3 ± 2.96	1082.68	Aggregated lumps and fused particles

| 2 | TMOS | 82.31 ± 3.84 | 94.5 ± 4.52 | 958.43 | Aggregated lumps and large particles |
| 3 | Sodium Silicate | 91.24 ± 4.51 | 65.2 ± 2.57 | 1193.56 | Fine powder with good flow property |

The particle size and surface area for all the silica sources were in the desirable range of below 100 nm and 1000 m²/g respectively. TEOS and TMOS yielded lumps, whereas in case of sodium silicate, the particles were uniform, powdery and free flowing (16).

6.2.6 Selection of base catalyst and role of pH in MSN synthesis

The pH of the reaction medium plays an important role in governing the particle size of MSNs. The particle size can be controlled by adding suitable base catalyst along with the alcohol. These agents alter the hydrolysis and condensation of silica precursor (17). They accelerate the reaction kinetics thus resulting in particles of smaller size. For the synthesis of MCM – 41 types of MSN, the solution is required to have basic pH, but for free flowing and monodispersed MSN, the pH should be below 12. The standard base catalysts NaOH and NH$_4$OH have been explored for formulation until now but it was observed that they yielded aggregated large particles due to rapid condensation and pH above 12 (14). The initial pH of the medium greatly affects the particle size of MSNs. When NH$_4$OH was used as a base catalyst, particle size increased with an increase in concentration of base. On increasing the concentration of NH$_4$OH beyond certain level (2%), the agglomeration of silica particles took place due to the increased ionic strength of the reaction medium (18).

Therefore, we used TEA as a base catalyst, as it has low condensation properties and low degree of amination, had the initial pH of 11, prevents the fusion and aggregation of nanoparticles, and controls the pore tunability. The results are displayed in Table 6.5.

Table 6.5 Selection of Base catalyst

Sr. No.	Base catalyst	%Yield	Reaction pH	Particle Size (nm)	Surface Area (m²/g)	Observation
1	NaOH	88.64 ± 3.59	13.6 ± 0.56	149.5 ± 6.32	896.25	Aggregated lumps and fused particles
2	NH₄OH	81.58 ± 2.86	12.8 ± 0.42	135.4 ± 5.18	994.63	Aggregated lumps and large particles
3	TEA	96.24 ± 3.71	10.8 ± 0.48	58.6 ± 1.09	1224.37	Fine powder with good flow property

6.3 Selection of excipient concentration

6.4.1 Effect of CTAB concentration

As presented in Table 6.6, increasing the concentration of CTAB resulted in increase of %yield, decrease in particle size of MSNs and subsequent increase in surface area up to concentration of 1% w/v (19). However, by increasing the concentration of CTAB more than 1% w/v, there was increase in particle size and decrease in surface area. This may be due to CTAB, a structure-directing template, promoting the hydrolysis of an alkoxide. During hydrolysis and condensation of an alkoxide, bromide ions of CTAB are exchanged for silicate anions at the CTAB micelle surface, which leads to rapid hydrolysis of the alkoxide, resulting in complete formation of mesoporous silica nanoparticles. However, in the case of CTAB below 1% w/v, too little CTAB may not be able to speed up the hydrolysis of alkoxide, resulting in incomplete formation and a low yield of mesoporous silica nanoparticles, increased particle size due to rod shaped particles and reduced surface area (20).

Table 6.6 Effect of CTAB concentration

Sr No.	Surfactant Concentration (%)	%Yield (%)	Size (nm)	Surface Area (m²/g)
1	0.25	54.63 ± 2.52	215.6 ± 7.4	652.18
2	0.5	68.96 ± 3.15	162.8 ± 6.3	812.65
3	0.75	82.35 ± 3.84	103.7 ± 4.1	923.24
4	1	93.18 ± 4.48	62.2 ± 1.8	1165.39
5	1.25	85.72 ± 3.19	139.4 ± 3.6	1036.58
6	1.5	73.81 ± 3.27	172.5 ± 5.7	836.43

6.3.2 Effect of silica source concentration

The amount of silica source is important in synthesis of Mesoporous Silica nanoparticles as it serves as silica precursor and affects the yield of MSN (21). A change from monodisperse (PDI: 0.067±0.004) to heterogenous particle size distribution (PDI: 0.598±0.051) was observed when the amount of sodium silicate was increased, which may be attributed to the secondary condensation reaction taking place due to the presence of excess silica precursor which starts producing new nuclei amongst the already existing silica particles (22).

Table 6.7 Effect of sodium silicate concentration

Sr No.	Silica Source Concentration (%)	%Yield (%)	Size (nm)	Surface Area (m²/g)
1	1	41.26 ± 1.65	168.6 ± 7.26	736.54
2	2	62.35 ± 2.53	135.1 ± 5.38	861.32
3	3	81.26 ± 3.38	105.3 ± 4.12	975.68
4	4	94.68 ± 4.24	68.5 ± 2.86	1168.92
5	5	82.65 ± 3.85	124.4 ± 3.54	1012.71
6	6	73.67 ± 3.12	158.2 ± 6.32	913.65

The %yield and surface area increased and particle size decreased up to silica concentration of 4% w/v, but particle size significantly increased above 4% w/v and surface area being inversely

proportional to particle size found to reduce and the %yield also reduced. Sodium silicate is the resource of the 'monomers' that forms the primary particles in the sol-gel system which will grow further to form the final product. Above that, TEA becomes the limiting reagent and not efficient in promoting condensation reactions (growth). The particles were relatively aggregated and widely distributed especially at higher concentrations of sodium silicate since excessive generation of primary particles at supersaturated concentration did not follow by sufficient consumption (low concentration of catalyst). These excess primary particles will spontaneously aggregate to form stable secondary particles, resulting in multi modal distribution and larger particle aggregates.

6.3.3 Effect of ethanol concentration

Presence of ethanol leads to formation of high quality, clear and uniform particles with desirable spherical morphology and smaller particles up to 100 nm in constant temperature (23). The increase in the amount of ethanol above 3 ml leads to the formation of larger silica particles with reduced surface area.

Table 6.8 Effect of ethanol concentration

Sr No.	Ethanol Concentration (%)	%Yield (%)	Size (nm)	Surface Area (m^2/g)
1	1	78.56 ± 3.54	125.6 ± 5.21	956.31
2	2	89.56 ± 4.25	85.3 ± 3.55	1085.63
3	3	93.62 ± 4.54	64.1 ± 2.65	1194.26
4	4	89.13 ± 3.74	92.3 ± 3.42	1036.52
5	5	88.72 ± 2.86	229.4 ± 4.16	876.28
6	10	85.61 ± 2.38	427.3 ± 6.24	575.16

Lower concentration of ethanol resulted in rapid evaporation as the reaction was carried out at higher temperature that led to negligible effect on reaction, increased particle size above 100 nm and low surface area, on increasing the ethanol concentration, the surface area tend to increase due to pore expansion and attainment of spherical shape that directly affects the surface area. With further increase in the amount of ethanol from 5 to 10, the particle size continues to grow with a diameter between 230 and 430 nm. This may be due to a combination

of (i) a very slow equilibrium toward the hydrolysis of TEOS due to solvation effects of the alcohol that influence the micelle formation, resulting in a slow growth of micelles on the surface of the center of the particles and (ii) a decrease in packing due to less tightly packed micelles (24).

6.3.4 Effect of Triethanolamine concentration

Triethanolamine in addition to base catalyst also acts as pore expanding agent. The higher concentration of TEA could give better surface capping of particles and prevented further growing of the nanoparticles. Besides, addition of TEA might accelerate of nuclei formation; therefore give larger number of particles (25).

Table 6.9 Effect of triethanolamine concentration

Sr No.	TEA concentration (w/w)	%Yield (%)	Size (nm)	Surface Area (m²/g)
1	1	58.56 ± 2.54	95.7 ± 5.21	963.58
2	2	89.74 ± 3.25	62.4 ± 3.55	1125.84
3	3	75.12 ± 4.54	124.1 ± 2.65	1023.29
4	4	66.13 ± 3.74	162.36 ± 3.42	863.12

At low concentration, the catalyst was unable to provide sufficient reaction catalysis and led to low yield. Based on the experimental results, we could deduce that the strong surface preventing effect of TEA reduced the growth rate of particles, and accelerate the nuclei formation, finally smaller sized MSNs with greater surface area were obtained, even though higher concentration of TEA above 2% w/v could accelerate the hydrolysis sodium silicate and promote the particle growth leading to increased particle size and reduced surface area. However, further increasing the dosage of TEA didn't reduce the diameters of MSNs anymore, which indicated that excessive amount of TEA will not affect the particle nucleation and growth of MSNs (7).

6.3.5 Selection of process parameters

The process parameters such as stirring time, stirring speed, condensation temperature, and rate of addition of silica source plays an important role on particle size, %yield, surface area and texture of silica nanoparticles.

6.10 Effect of process parameters on particle size, surface area and %yield

Effect of process parameters on quality of mesoporous silica nanoparticles			
Stirring speed (rpm)	**%Yield (%)**	**Size (nm)**	**Surface Area (m²/g)**
300	48.72 ± 2.18	218.6 ± 8.5	655.24
600	57.28 ± 2.24	165.1 ± 6.3	771.85
900	68.25 ± 3.12	118.3 ± 2.2	984.62
1200	89.21 ± 3.69	68.6 ± 1.5	1159.15
1500	78.18 ± 2.58	113.2 ± 2.9	1026.32
Stirring time (H)	**%Yield (%)**	**Size (nm)**	**Surface Area (m²/g)**
0.5	54.68 ± 1.51	156.1 ± 3.8	884.56
1	62.31 ± 2.64	122.3 ± 2.3	976.28
2	91.84 ± 2.89	76.6 ± 1.9	1128.32
3	83.14 ± 3.61	116.8 ± 2.1	1034.21
4	72.38 ± 2.94	132.2 ± 3.4	912.34
Temperature (°C)	**%Yield (%)**	**Size (nm)**	**Surface Area (m²/g)**
50	58.24 ± 2.84	141.6 ± 2.5	915.43
60	71.31 ± 3.18	124.2 ± 1.9	998.22
70	79.43 ± 2.68	96.2 ± 1.4	1087.65
80	93.68 ± 3.24	67.6 ± 1.5	1181.52
90	82.18 ± 2.65	108.6 ± 1.2	1074.68
100	71.62 ± 3.84	136.2 ± 1.8	965.18
Rate of addition	**%Yield (%)**	**Size (nm)**	**Surface Area (m²/g)**
Flash addition	84.56 ± 3.65	152.3 ± 5.62	965.23
1 ml/min	95.24 ± 4.25	65.4 ± 2.35	1163.25
2 ml/min	79.65 ± 3.51	129.64 ± 3.68	1013.84

6.3.5.1 Stirring Speed

Stirring speed in the range of 300 to 1500 rpm was screened. With increase in stirring speed up to 1200 rpm the particle size decreased and % yield and surface increased. At low-speed, adequate mixing of the formulation components was not attained, as TEA was viscous in nature, and it required higher shear to attain equilibrium between components that led to particle size below 100 nm and %yield above 80%. Above 1200 rpm, at 1500 rpm, due to excess shear, the surfactant formed bubbles that led to excess air entrapment and retention of surfactant on the surface of reaction mixture that reduced the yield and increased particle size due to interference of globules.

6.3.5.2 Stirring Time

Stirring time plays a crucial role in bringing about condensation and progression of reaction. Increasing the stirring time up to 2 hrs., increased the yield and reduced the particle size, as at lower reaction time there was incomplete condensation that led to reduction in yield and increase in particle size was observed. After 2 hrs., there was significant reduction in water volume that increased the viscosity leading to formation of fused nanoparticles with higher particle size and lower yield.

6.3.5.3 Temperature

Reaction temperature is one of the most important formulation parameters for synthesis of silica nanoparticles. Temperature below 80°C was found to be inadequate to bring about the condensation of the reaction mixture, leading to low %yield and surface area and higher particle size. The particle sizes of MSNs decreased from 140 nm to 68 nm with the elevating of reaction temperature from 50°C to 80°C. Above 80°C the hydrodynamic particle size of MSNs increases with the elevation of reaction temperature, as high temperature accelerates the rates of sodium silicate hydrolysis and silica monomer generation, which results in growth of nanoparticles and further formation of larger sizes MSNs.

6.3.5.4 Rate of addition

Slower addition of TEA and sodium silicate resulted in smaller particle size while faster addition will result in bigger particles since the catalyst feed rate directly influences the reaction rate. Addition rate of 1 ml/ min produced homogenous and narrow distributed particles. This is due to extended induction period which generates primary particles at slower rate and in turn the rate of growth was also being slowed down. Faster addition rate above 1 ml/ min and flash

addition resulted in rapid formation and consumption of monomeric species that further increased nucleation and reduced condensation, leading to increase in particle size

6.4 Plackett-Burman design for screening study (Primary design):

The results of preliminary study were useful to identify formulation-related and process-related parameters and to understand the source of variables to improve the quality of product to assist formulation and process. Key product attributes recognized as particle size, surface area and % yield were evaluated for different variables. The goals of applying design were to achieve the highest % yield, surface area and lowest particle size.

Table 6.11 Variables and levels selected for preliminary study

Factor	Name	Unit	Low actual	High actual
A	Surfactant Concentration	%	0.25	1.5
B	Silica Source Concentration	%	1	5
C	TEA Concentration	w/w	1	4
D	Ethanol Concentration	%	1	5
E	Stirring Speed	rpm	300	1500
F	Stirring time	H	0.5	4
G	Stirring Temperature	°C	50	100

Table 6.12 Design Matrix of Plackett Burman Design

Run	Factor A Surfactant Concentration (%)	Factor B Silica Source Concentration (%)	Factor C TEA Concentration (w/w)	Factor D Ethanol Concentration (%)	Factor E Stirring speed (rpm)	Factor F Stirring Time (H)	Factor G Stirring Temp. (°C)	Response-1 Particle Size (nm)	Response-2 %Yield (%)	Response – 3 Surface area (m²/g)
1	0.25	5.00	4.00	5.00	300.00	0.50	50.00	221.5	712.3	59.84
2	0.25	1.00	1.00	1.00	300.00	0.50	50.00	124.6	1062.4	82.36
3	0.25	1.00	4.00	1.00	1500.00	4.00	50.00	165.7	825.1	69.52
4	1.50	5.00	1.00	1.00	300.00	4.00	50.00	112.3	1098.1	87.31
5	0.25	1.00	1.00	5.00	300.00	4.00	100.00	167.5	802.5	71.26
6	1.50	5.00	4.00	1.00	300.00	0.50	100.00	92.6	1124.8	91.54
7	1.50	5.00	1.00	5.00	1500.00	4.00	50.00	152.3	912.5	74.56
8	0.25	5.00	1.00	5.00	1500.00	0.50	100.00	175.8	864.1	68.54
9	0.25	5.00	4.00	1.00	1500.00	4.00	100.00	132.4	994.5	78.61
10	1.50	1.00	4.00	5.00	1500.00	0.50	50.00	125.4	1035.4	84.26
11	1.50	1.00	1.00	1.00	1500.00	0.50	100.00	85.2	1253.2	96.52
12	1.50	1.00	4.00	5.00	300.00	4.00	100.00	116.2	1084.6	89.54

6.4.1.1 ANOVA for particle size

Multi-linear regression analysis and ANOVA (shown in Table 6.13) have been performed to analyse the data, and a series of Pareto charts were constructed to demonstrate the influence of each parameter on particle size.

Table 6.13 ANOVA for particle size (Factorial model)

Source	Sum of squares	Degree of Freedom	Mean square	F – Value	p-value (prob>F)
Model	15603.84	6	2600.64	13.35	0.0060
A-Surfactant Concentration	7676.02	1	7676.02	39.42	0.0015
B-Silica Source concentration	372.00	1	372.00	1.91	0.2255
C-TEA Concentration	313.35	1	313.35	1.61	0.2605
D-Ethanol concentration	5038.90	1	5038.90	25.88	0.0038
G-Stirring Temp	1879.98	1	1879.98	9.65	0.0266
A&D	454.01	1	454.01	2.33	0.1873
Model Statistics					
Standard Deviation	13.95				
Mean	139.29				
R^2	0.9413				
Adequate Precision	13.292				

The Model F-value of 13.35 implies the model is significant. There is only a 0.60% chance that a "Model F-Value" this large could occur due to noise. Values of "Prob > F" less than 0.0500 indicate model terms are significant. In this case A, D, G are significant model terms. Values greater than 0.1000 indicate the model terms are not significant. Theadequate precision of 13.292 indicates an adequate signal. Hence we can conclude that the Surfactant concentration (A), Ethanol concentration and Stirring temperature (G) are the potential factors that affect the particle size.

6.4.1.2 Influence of factors on particle size (Pareto Chart)

As represented in Figure 6.1, factor A (Surfactant concentration) and factor D (Ethanol concentration) had crossed the Bonferroni limit and possessed the utmost importance for

reducing particle size and factor G (stirring temperature) may have an immediate effect on the particle size as the factor crosses the t-critical value limit.
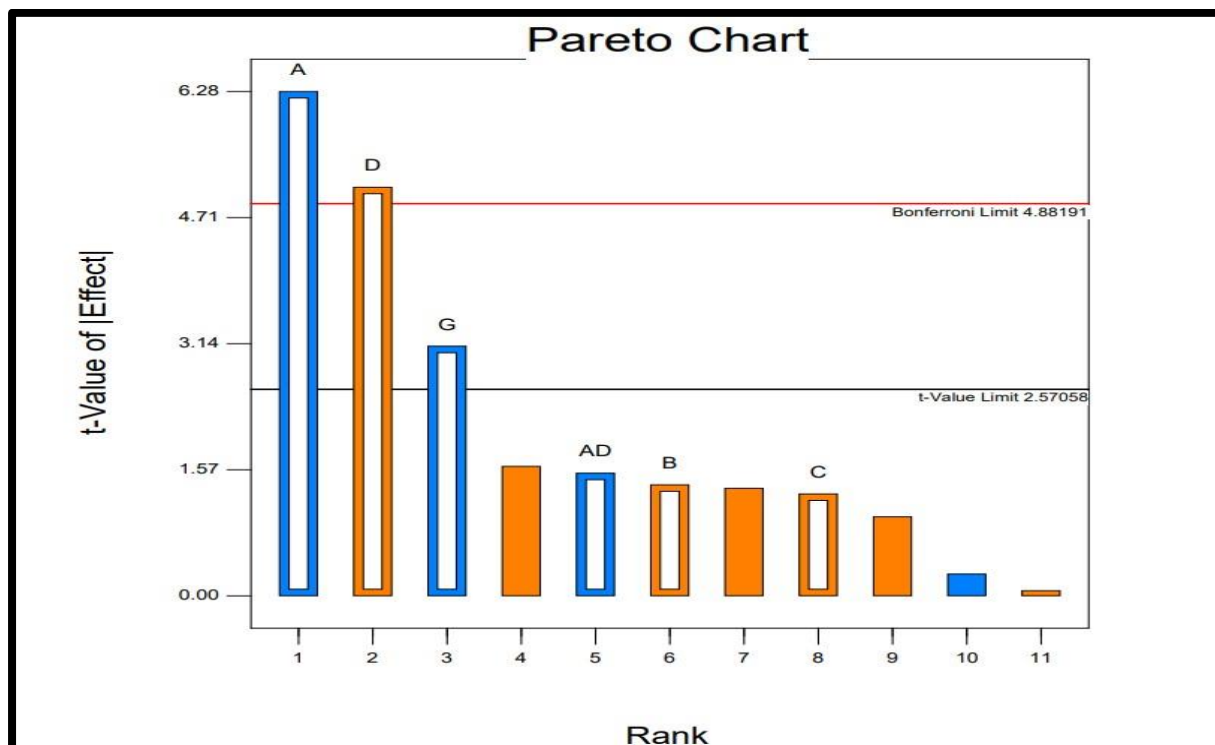
**Figure 6.1 Pareto Chart for the selected factorial model particle size**

The Pareto chart depicted that the independent variables viz. surfactant concentration, ethanol concentration and stirring speed have exerted most significant effect (Above t-value limit) on the response variables.

6.4.1.3 ANOVA for Surface area (Factorial model)

Multi-linear regression analysis and ANOVA (shown in Table 6.14) have been performed to analyse the data, and a series of Pareto charts were constructed to demonstrate the influence of each parameter on the surface area.

Table 6.14 ANOVA on factorial model for surface area

Source	Sum of squares	Degree of Freedom	Mean square	F – Value	p-value (prob>F)
Model	260611.05	6	43428.65	14.35	0.0051
A-Surfactant Concentration	80626.04	1	80626.04	26.63	0.0036

B-Silica Source concentration	10614.80	1	10614.80	3.51	0.1200
D-Ethanol concentration	41412.91	1	41412.91	13.68	0.0140
F-Stirring time	9346.50	1	9346.50	3.09	0.1392
G-Stirring Temp	31413.57	1	31413.57	10.38	0.0234
B&F	17161.87	1	17161.87	5.67	0.0631
Model Statistics					
Standard Deviation		55.02			
Mean		980.79			
R^2		0.9451			
Adequate Precision		13.484			

The Model F-value of 14.35 implies the model is significant. There is only a 0.51% chance that a "Model F-Value" this large could occur due to noise. Values of "Prob > F" less than 0.0500 indicate model terms are significant. In this case A, D, G are significant model terms. Values greater than 0.1000 indicate the model terms are not significant. The adquate precision of 13.484 indicates an adequate signal. Hence we can conclude that the Surfactant concentration (A), Ethanol concentration and Stirring temperature (G) are the potential factors that affect the surface area.

6.4.1.4 Influence of factors on surface area (Pareto Chart)

As represented in Figure 6.2, factor A (Surfactant concentration) had crossed the Bonferroni limit and possessed the utmost importance for increasing surface area and factor D (Ethanol concentration) and factor G (stirring temperature) may have an immediate effect on the surface area as the factor crosses the t-critical value limit.
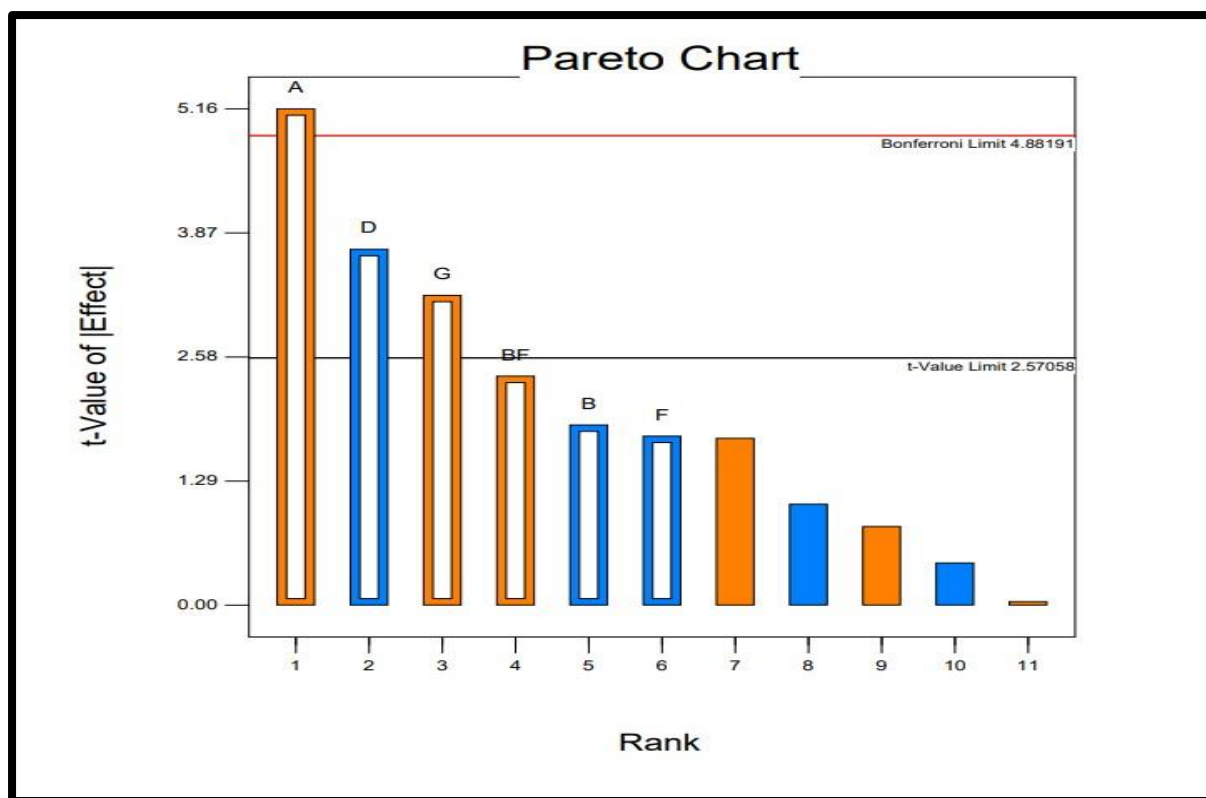
Figure 6.2 Pareto chart for a selected factorial model of surface area

6.4.1.5 ANOVA for %Yield (Factorial model)

Multi-linear regression analysis and ANOVA (shown in Table 6.15) have been performed to analyse the data, and a series of Pareto charts were constructed to demonstrate the influence of each parameter on the % yield.

Table 6.15 ANOVA on factorial model for %yield

Source	Sum of squares	Degree of Freedom	Mean square	F – Value	p-value (prob>F)
Model	1287.16	7	183.88	18.64	0.0066
A-Surfactant Concentration	525.75	1	525.75	53.31	0.0019
B-Silica Source concentration	113.11	1	113.11	11.47	0.0276
D-Ethanol concentration	201.55	1	201.55	20.44	0.0107
F-Stirring time	12.53	1	12.53	1.27	0.3228
G-Stirring Temp	173.58	1	173.58	17.60	0.0137

Model Statistics	
Standard Deviation	3.14
Mean	79.49
R^2	0.9703
Adequate Precision	15.489

The Model F-value of 18.64 implies the model is significant. There is only a 0.66% chance that a "Model F-Value" this large could occur due to noise. Values of "Prob > F" less than 0.0500 indicate model terms are significant. In this case A, B, D, G are significant model terms. Values greater than 0.1000 indicate the model terms are not significant. The adequate precision of 15.489 indicates an adequate signal. Hence we can conclude that the Surfactant concentration (A),Silica source concentration (B), Ethanol concentration and Stirring temperature (G) were the potential factors that affected the %yield.

6.4.1.6 Influence of factors on %yield (Pareto Chart)

As represented in Figure 6.3, factor A (Surfactant concentration) had crossed the Bonferroni limit and possessed the utmost importance for increasing %yield and factor B (Silica concentration), factor D (Ethanol concentration), and factor G (stirring temperature) may have an immediate effect on the %yield as the factor crosses the t-critical value limit.
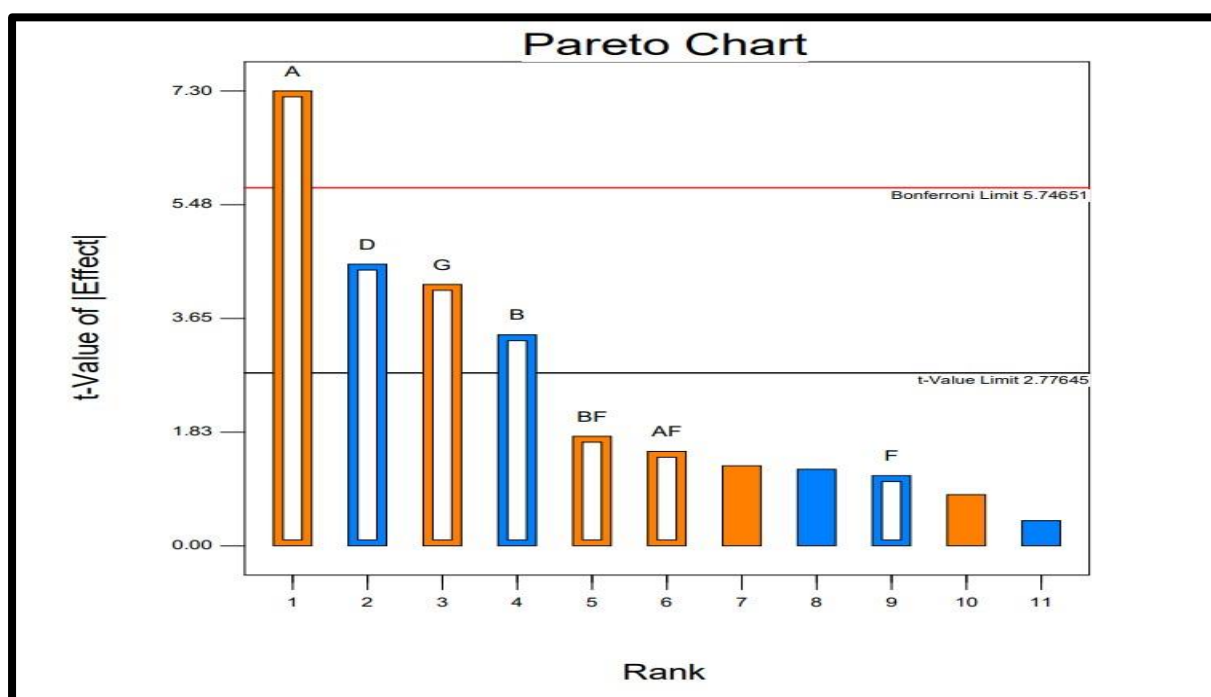
Figure 6.3 Pareto chart for a selected factorial model of %yield

6.4.2 Box Behnken design for point prediction (Secondary design)

Based on the results of the primary factor screening design, three variables (i.e., surfactant concentration, silica source concentration and stirring temperature) were selected for further optimization (Table 6.16) using Box-Behnken design (26).

Table 6.16 Variables and levels selected based on primary design

Independent variables	Unit	Levels	
		-1	+1
A: Surfactant concentration	%	0.6	1.8
B: Silica source concentration	%	2	6
C: Stirring Temperature	°C	60	100
Dependent variables	Unit		
1. Particle size	nm		
2. Surface area	m^2/g		
3. %Yield	%		

Table 6.17 Design matrix of Box -Behnken Design

Run	Factor A Surfactant Concentration (%)	Factor B Silica Source Concentration (%)	Factor C Stirring Temperature (°C)	Response – 1 Particle Size (nm)	Response – 2 Surface Area (m^2/g)	Response – 3 % Yield (%)
1	1.80	4.00	60.00	163.2	911.23	66.53
2	0.60	2.00	80.00	131.5	1012.35	76.52
3	0.60	4.00	100.00	95.8	1123.62	87.56
4	0.60	4.00	60.00	152.3	928.61	69.52
5	1.20	6.00	60.00	128.6	1025.65	76.52
6	1.20	4.00	80.00	68.6	1238.23	93.62
7	1.20	4.00	80.00	69.4	1217.54	92.16
8	1.20	2.00	60.00	156.2	945.63	72.65

9	1.20	2.00	100.00	135.1	982.12	74.23
10	1.20	6.00	100.00	122.3	1068.25	82.75
11	1.80	6.00	80.00	165.2	916.25	69.56
12	0.60	6.00	80.00	136.9	958.63	73.65
13	1.80	4.00	100.00	195.2	824.56	64.56
14	1.80	2.00	80.00	214.6	701.32	55.63
15	1.20	4.00	80.00	67.8	1253.87	95.23

6.4.2.1 Statistical analysis of response: Particle Size

6.4.2.1.1 ANOVA results of different models

Multi-linear regression analysis and ANOVA (Table 6.1) have been performed to analyse the data, and a series of response surface plots were constructed to demonstrate the influence of each parameter on particle size of MSNs.

Table 6.18 Summary of ANOVA results of different models for Particle Size

Source	Sequential p-value	Lack of fit p-value	Adjusted R-Squared	Predicted R-Squared	Suggested model
Linear	0.3081	0.0003	0.0701	-0.1057	
2FI	0.6056	0.0002	0.3703	-0.4253	
Quadratic	<0.0001	0.4293	0.9996	0.9982	Suggested
Cubic	0.0003	0.2526	0.9997		Aliased

Highest polynomial showing the lowest p value (<0.05) along with highest Lack of Fit p-value (>0.1) was considered for model selection. Based on the criteria, quadratic model was found to be best fit to the observed responses (Table 6.18).

Table 6.19 ANOVA results of quadratic mixture model for Particle Size

Source	Sum of Squares	Df	Mean Square	F – Value	p-value Prob > F	
Model	27361.87	9	3040.21	3705.31	< 0.0001	Significant
A-Surfactant Concentration	6143.86	1	6143.86	7487.95	< 0.0001	
B-Silica Source concentration	890.42	1	890.42	1085.22	< 0.0001	
C-Stirring Temperature	336.70	1	336.70	410.36	< 0.0001	
AB	750.76	1	750.76	915.00	< 0.0001	
AC	1958.06	1	1958.06	2386.43	< 0.0001	
BC	54.76	1	54.76	66.74	0.0004	
A^2	11072.98	1	11072.98	13495.40	< 0.0001	
B^2	5526.36	1	5526.36	6735.36	< 0.0001	
C^2	2949.30	1	2949.30	3594.52	< 0.0001	
Residual	4.10	5	0.82			
Lack of Fit	2.82	3	0.94	1.47	0.4293	not significant
Pure Error	1.28	2	0.64			
Cor Total	27365.98	14				

ANOVA Summary				
Parameters	**Results**	**Parameters**		**Results**
Std. Dev.	0.91	R – Squared		0.9999
Mean	133.51	Adj. R – Squared		0.9996
C.V %	0.68	Pred R – Squared		0.9982
Press	48.04	Adeq. Precision		196.611

The ANOVA table revealed that the effect of factors was significant and hence the model is significant for the particle size. The F-value was the highest for factor A (7487.95), i.e., increasing the surfactant concentration would decrease the particle size of silica nanoparticles in quadratic manner. Other two factors, silica source concentration (factor B) and stirring

temperature (factor C) have lower but significant effect on particle size which can also be observed from the surface plots.

The Model F-value of 3705.31 implies the model is significant. There is only a 0.01% chance that a "Model F-Value" this large could occur due to noise. Values of "Prob > F" less than 0.0500 indicate model terms are significant. In this case A, B, C, AB, AC, BC, A^2, B^2, C^2 are significant model terms. Values greater than 0.1000 indicate the model terms are not significant. The "Lack of Fit F-value" of 1.47 implies the Lack of Fit is not significant relative to the pure error. There is a 42.93% chance that a "Lack of Fit F-value" this large could occur due to noise. The "Pred R-Squared" of 0.9982 is in reasonable agreement with the "Adj R-Squared" of 0.9996. The adequate precision of 196.611 indicates an adequate signal. This model can be used to navigate the design space.

6.4.2.1.2 Model diagnostic plots for particle size.

6.4.2.1.2.1 Normal residual plot

In this case, as the plot looks to fit in fat pencil (Figure 6.4) it is considered as normal.
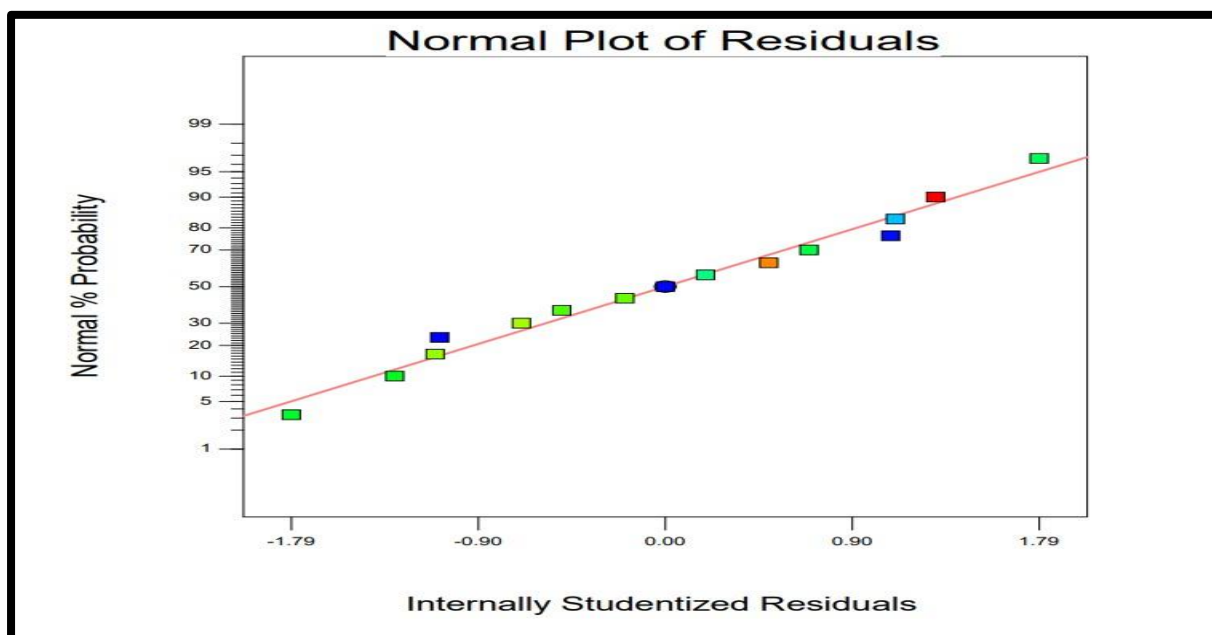
Figure 6.4 Normal plot of residuals for particle Size

6.4.2.1.2.2 Residuals vs Predicted plot

The responses in Figure 6.5 showed the distribution of variance throughout the design space and it did not follow any specific pattern indicating the random distribution of variance and randomization of predicted value to residual values.
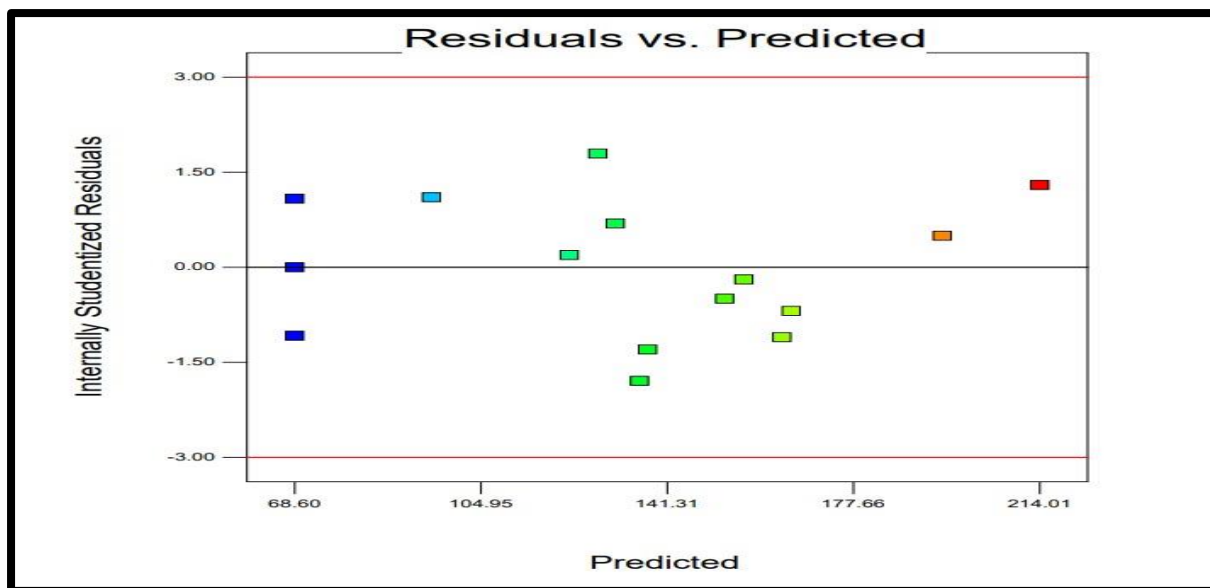
Figure 6.5 Residual vs Predicted plot for particle size

6.4.2.1.2.3 Residual vs Run order plot

The residual vs run data for particle size (Figure 6.6) is having a random scatter of residuals which indicate there is no time dependent changes occurring in the residuals. The points plotted in random plot doesn't follow a fixed pattern of runs, which explains the randomization of design carried out for identification of independent variables on dependent responses.
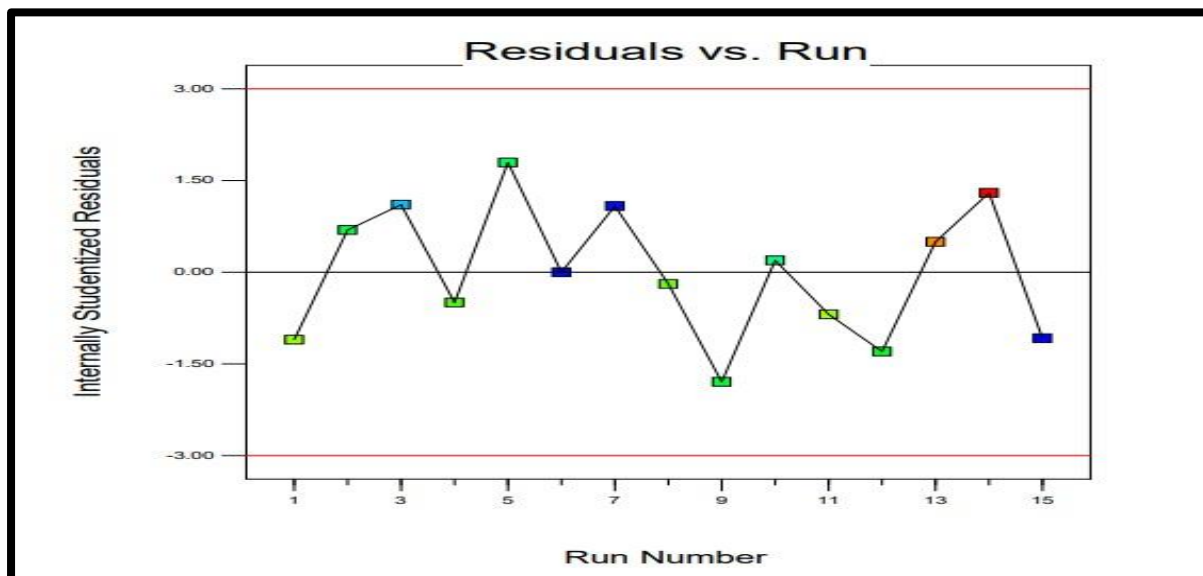
Figure 6.6 Residual vs Run order plot for particle size

6.4.2.1.2.4 Predicted vs Actual plot

The actual points followed an angle of 45° (Figure 6.7) and none of the point was found to variate from linearity, so the plot of predicted vs actual points proved the data to be free from error as well as bias.
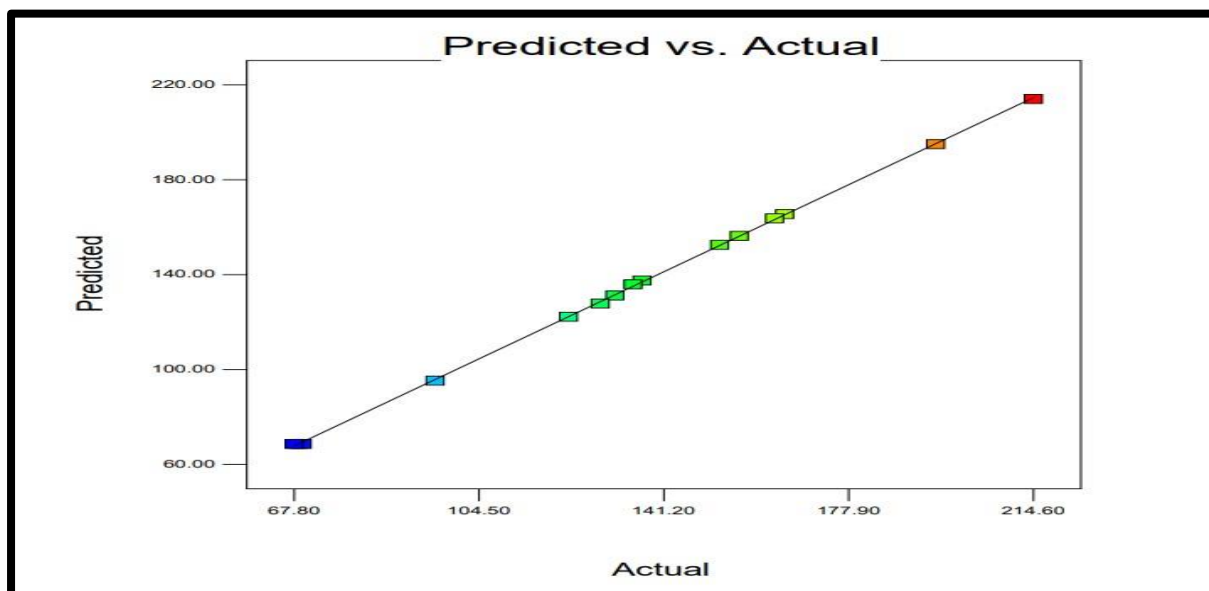
Figure 6.7 Predicted vs Actual plot for particle size

6.4.2.1.2.5 Box-Cox plot for power transformation

Plot in Figure 6.8 shows the λ value of 1, which lies near the best λ value and within 95% confidence interval, indicating no requirement for any data transition.
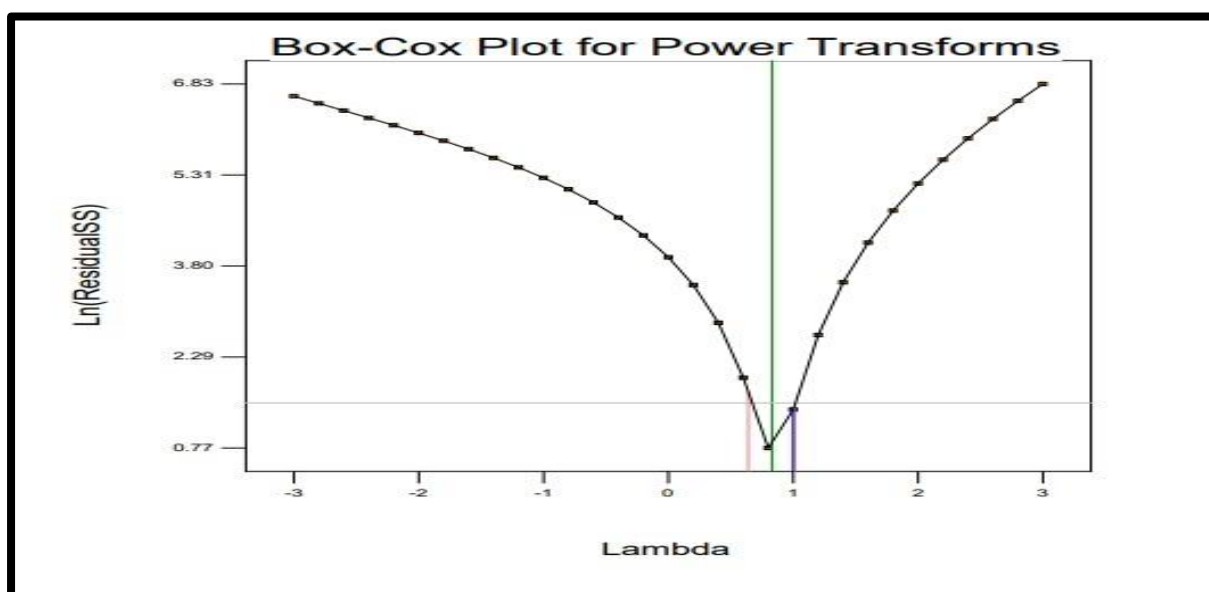
Figure 6.8 Box Cox plot for power transformation for particle size

6.4.2.1.2.6 Piepel's plot

A steep slope for factor A (surfactant concentration) and curvature for factor B (silica source concentration) and factor C (stirring temperature) as shown in figure 6.9 proves that response was sensitive to the factors. The line for surfactant concentration shows sharp deviation from normal which suggests that it had a great impact on particle size.
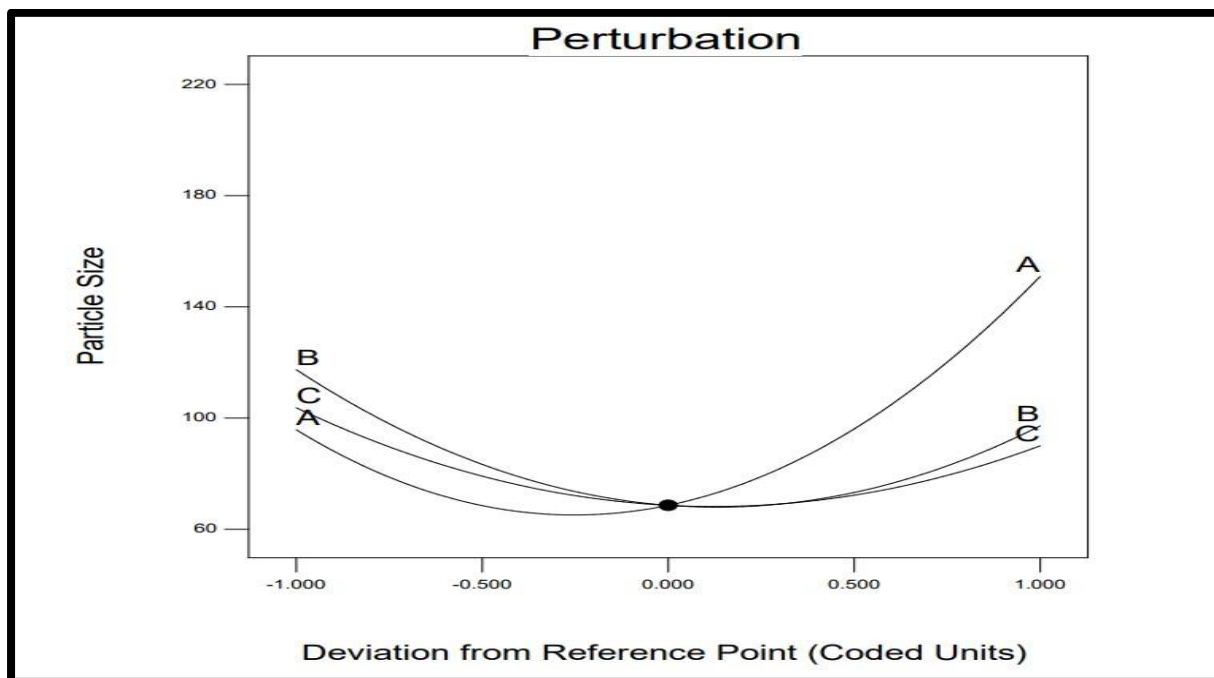
Figure 6.9 Piepel's Plot

6.4.2.1.2.7 Response surface (3D) plots

The RED area in the Figure 6.10 shows the area of maximum particle size and BLUE zone represents the area with lowest particle size.
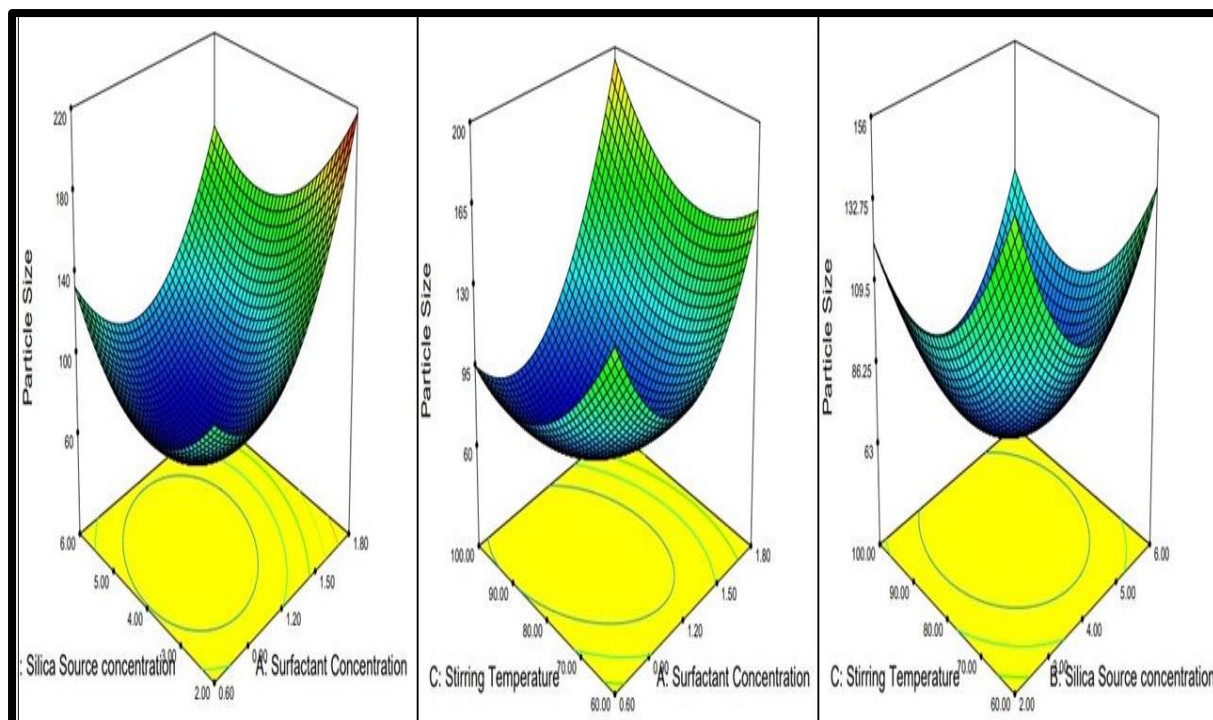
Figure 6.10 Response surface (3D) plots for particle size

Two-factor 3D response surface plots for particle size justifies the significant terms. A quadratic model was found to be best fit with the applied design and the higher cubic model was found to be aliased. From the plots, it can be concluded that increasing the surfactant concentration and silica source concentration initially decreased the particle size but from a certain point the particle size increased. This may be due to increased foaming of the solution that did not allow the silica and TEA to interact and leading to settling of sodium silicate, and increased viscosity of system that increases the particle size.

6.4.2.1.3 Mathematical equation for particle size

Final equation in terms of coded factors has been obtained as below:

$$\textbf{Particle Size} = +68.60 + 27.71*A - 10.55*B - 6.49*C - 13.70*A*B* + 22.13*A*C + 3.70*B*C + 54.76*A^2 + 38.69*B^2 + 28.26*C^2 \text{--------- (6.1)}$$

6.4.2.2 Statistical analysis of response: Surface area

6.4.2.2.1 ANOVA results of different models

Multi-linear regression analysis and ANOVA (Table 6.20) have been performed to analyse the data, and a series of response surface plots were constructed to demonstrate the influence of each parameter on surface area of MSNs.

Table 6.20 Summary of ANOVA results of different models for surface area

Source	Sequential p-value	Lack of fit p-value	Adjusted R-Squared	Predicted R-Squared	Suggested Model
Linear	0.4117	0.0115	0.0092	-0.1949	
2FI	0.6768	0.0090	-0.1635	-0.5553	
Quadratic	<0.0001	0.8380	0.9921	0.9820	Suggested
Cubic	0.0119	0.5477	0.9861		Aliased

Highest polynomial showing the lowest p value (<0.05) along with highest Lack of Fit p-value (>0.1) was considered for model selection. Based on the criteria, quadratic model was found to be best fit to the observed responses (Table 6.20).

Table 6.21 ANOVA results of quadratic mixture model for surface area

Source	Sum of Squares	Df	Mean Square	F – Value	p-value Prob > F	
Model	332550.51	9	36947.10	195.48	<0.0001	Significant
A-Surfactant Concentration	56087.38	1	56087.38	296.75	< 0.0001	
B-Silica Source concentration	13395.57	1	13395.57	70.87	0.0004	
C-Stirring Temperature	4391.25	1	4391.25	23.23	0.0048	
AB	18043.21	1	18043.21	95.46	0.0002	
AC	19835.91	1	19835.91	104.95	0.0002	
BC	9.33	1	9.33	0.049	0.8329	
A^2	146100	1	146100	772.91	<0.0001	
B^2	72887.94	1	72887.94	385.64	< 0.0001	
C^2	30330.10	1	30330.10	160.47	< 0.0001	
Residual	945.03	5	189.01			
Lack of Fit	280.84	3	93.61	0.28	0.8380	not significant
Pure Error	664.18	2	332.09			

Cor Total	335000	14				
ANOVA Summary						
Parameters	**Results**		**Parameters**		**Results**	
Std. Dev.	13.75		R – Squared		0.9972	
Mean	1007.19		Adj. R – Squared		0.9921	
C.V %	1.36		Pred R – Squared		0.9820	
Press	5987.91		Adeq. Precision		47.324	

The ANOVA table revealed that the effect of factors was significant and hence the model is significant for the surface area. The F value was the highest for the factor A (296.75), i.e., increasing the surfactant concentration increases the surface area in quadratic manner, but further increase in concentration it lead to encapsulation of surfactant molecule in its core that led to reduction in surface area. Surfactant concentration had most prominent effect as their p-value is <0.0001. The other factors, silica source concentration (factor B) and stirring temperature (factor C) too have significant effect but less compared to surfactant concentration.

The Model F-value of 195.48 implies the model is significant. There is only a 0.01% chance that a "Model F-Value" this large could occur due to noise. Values of "Prob > F" less than 0.0500 indicate model terms are significant. In this case A, B, C, AB, AC, A^2, B^2, C^2 are significant model terms. Values greater than 0.1000 indicate the model terms are not significant. The "Lack of Fit F-value" of 0.28 implies the Lack of Fit is not significant relative to the pure error. There is a 83.80% chance that a "Lack of Fit F-value" this large could occur due to noise. The "Pred R-Squared" of 0.9820 is in reasonable agreement with the "Adj R-Squared" of 0.9921. The adequate precision of 47.324 indicates an adequate signal. This model can be used to navigate the design space.

6.4.2.2.2 Model diagnostics plots for surface area

6.4.2.2.2.1 Box Cox plot for power transformation

Figure 6.11 shows the λ value of 1, which lies near the best λ value and within 95% confidence interval, indicating no requirement for any data transition.
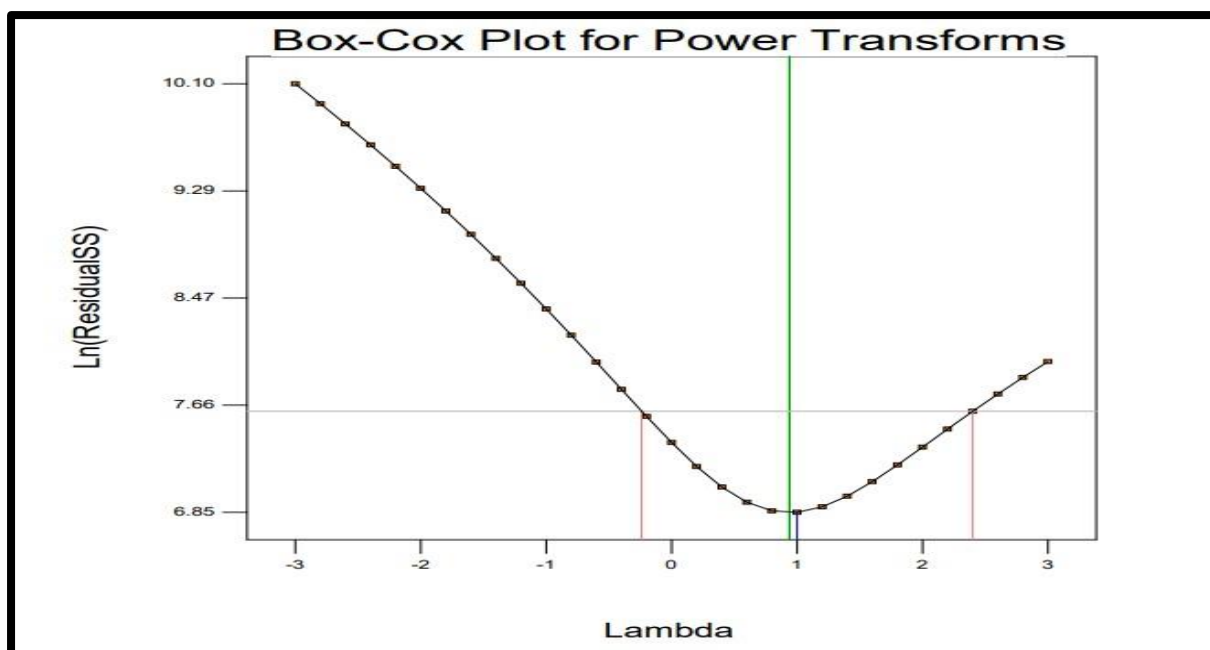
Figure 6.11 Box Cox plot for power transformation for surface area

6.4.2.2.2 Piepel's plot

A steep slope for factor A (surfactant concentration) and curvature for factor B (silica source concentration) and factor C (stirring temperature) as shown in figure 6.12 proves that response was sensitive to the factors. The line for surfactant concentration shows sharp deviation from normal which suggests that it had a great impact on surface area.
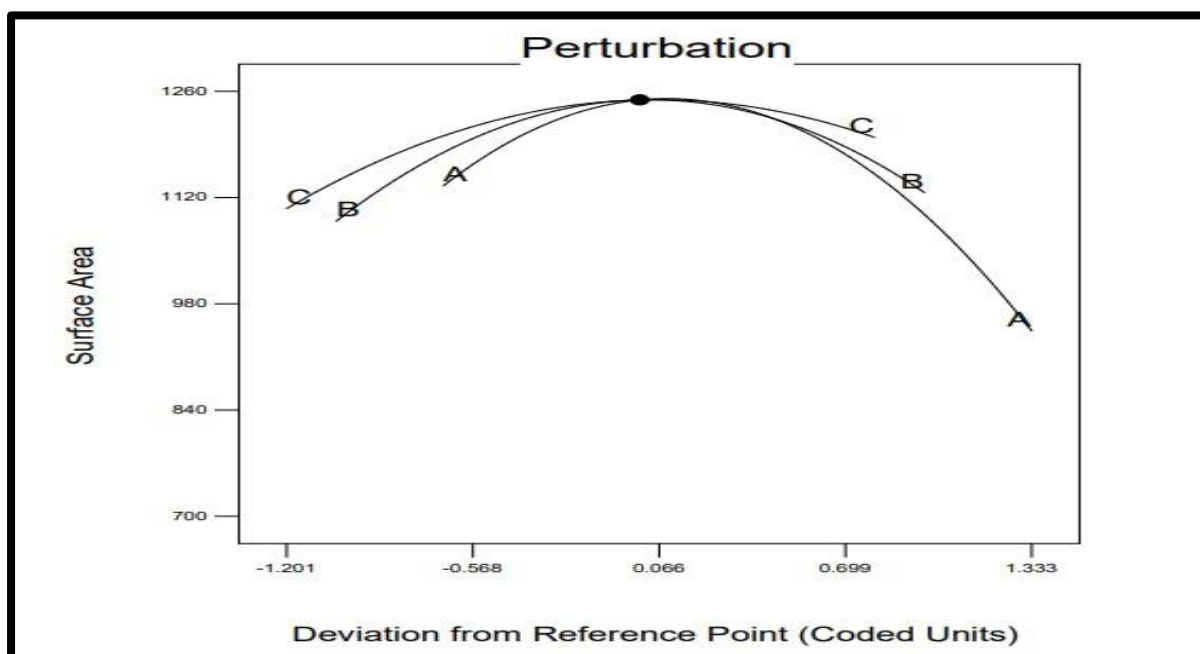

Figure 6.12 Piepel's plot

6.4.2.2.2.3 Response surface (3D) plots

The RED area in the Figure 6.12 shows the area of maximum surface area and BLUE zone represents the area with lowest surface area.
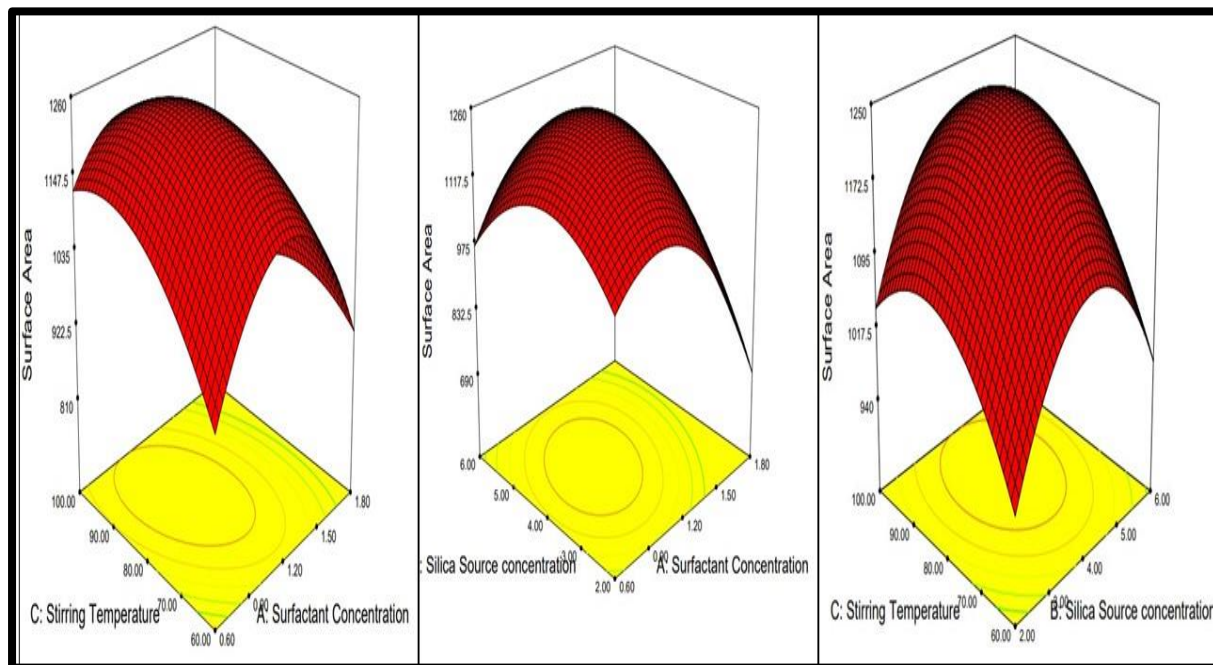
Figure 6.13 Response surface (3D) plot for surface area

Two-factor 3D response surface plots for surface area justifies the significant terms. A quadratic model was found to be best fit with the applied design and the higher cubic model was found to be aliased. From the plots, it can be concluded that increasing the surfactant concentration and silica source concentration initially increases the surface area but from a certain point the surface area decreases. This may be due to increased surfactant incorporation in the pores of silica nanoparticles and incomplete formation of nanoparticles that lead to reduction in surface area of MSNs

6.4.2.2.3 Mathematical equation for surface area

Surface area = $+1265.55 - 83.73*A + 40.92*B + 23.43*C + 67.16*A*B - 70.42*A*C + 1.53*B*C - 198.91*A^2 - 140.50*B^2 - 90.63*C^2$ -------- **(6.2)**

6.4.2.3 Statistical analysis of response: %Yield

6.4.2.3.1 ANOVA results of different models

Multi-linear regression analysis and ANOVA (Table 6.22) have been performed to analyse the data, and a series of response surface plots were constructed to demonstrate the influence of each parameter on % yield of MSNs.

Table 6.22 Summary of ANOVA results of different models for % yield

Source	Sequential p-value	Lack of fit p-value	Adjusted R-Squared	Predicted R-Squared	Suggested Model
Linear	0.3458	0.0152	0.0466	-0.1390	
2FI	0.6552	0.0116	-0.1446	-0.5270	
Quadratic	<0.0001	0.4723	0.9795	0.9176	Suggested
Cubic	0.0152	0.1976	0.9822		Aliased

Highest polynomial showing the lowest p value (<0.05) along with highest Lack of Fit p-value (>0.1) was considered for model selection. Based on the criteria, quadratic model was found to be best fit to the observed responses (Table 6.22).

Table 6.23 ANOVA results of quadratic mixture model for %yield

Source	Sum of Squares	Df	Mean Square	F – Value	p-value Prob > F	
Model	1838.76	9	204.31	75.15	<0.0001	Significant
A-Surfactant Concentration	324.74	1	324.74	119.45	0.0001	
B-Silica Source concentration	68.74	1	68.74	25.28	0.0040	
C-Stirring Temperature	71.28	1	71.28	26.22	0.0037	
AB	70.56	1	70.56	25.95	0.0038	
AC	100.10	1	100.10	36.82	0.0018	
BC	5.41	1	5.41	1.99	0.2176	
A^2	793.81	1	793.81	291.98	<0.0001	

B^2	381.70	1	381.70	140.40	<0.0001	
C^2	179.12	1	179.12	65.88	0.0005	
Residual	13.59	5	2.72			
Lack of Fit	8.88	3	2.96	1.25	0.4723	not significant
Pure Error	4.72	2	2.36			
Cor Total	1852.35	14				

ANOVA Summary			
Parameters	**Results**	**Parameters**	**Results**
Std. Dev.	1.65	R – Squared	0.9927
Mean	76.71	Adj. R – Squared	0.9795
C.V %	2.15	Pred R – Squared	0.9176
Press	152.64	Adeq. Precision	28.473

The ANOVA table revealed that the effect of factors was significant and hence the model is significant for the %yield. The F value was the highest for the factor A (119.45), i.e., increasing the surfactant concentration will increase the %yield in quadratic manner and had the most prominent effect as its p-value is 0.0001. With increasing the surfactant concentration, the yield increased but as it reached the threshold, the yield starts decreasing since there was bubbling that occupied the space and there was inadequate mixing between formulation components that lead to incomplete reaction resulting in low yield. Other factors silica source concentration and stirring temperature had less significant effect compared to surfactant concentration.

The Model F-value of 75.15 implies the model is significant. There is only a 0.01% chance that a "Model F-Value" this large could occur due to noise. Values of "Prob > F" less than 0.0500 indicate model terms are significant. In this case A, B, C, AB, AC, A^2, B^2, C^2 are significant model terms. Values greater than 0.1000 indicate the model terms are not significant. The "Lack of Fit F-value" of 1.25 implies the Lack of Fit is not significant relative to the pure error. There is a 47.23% chance that a "Lack of Fit F-value" this large could occur due to noise. The "Pred R-Squared" of 0.9176 is in reasonable agreement with the "Adj R-Squared" of 0.9795. The adequate precision of 28.473 indicates an adequate signal. This model can be used to navigate the design space.

6.4.2.3.2 Model diagnostic plots for % yield

6.4.2.3.2.1 Box – Cox plot

Figure 6.14 shows the λ value of 1, which lies near the best λ value and within 95% confidence interval, indicating no requirement for any data transition.
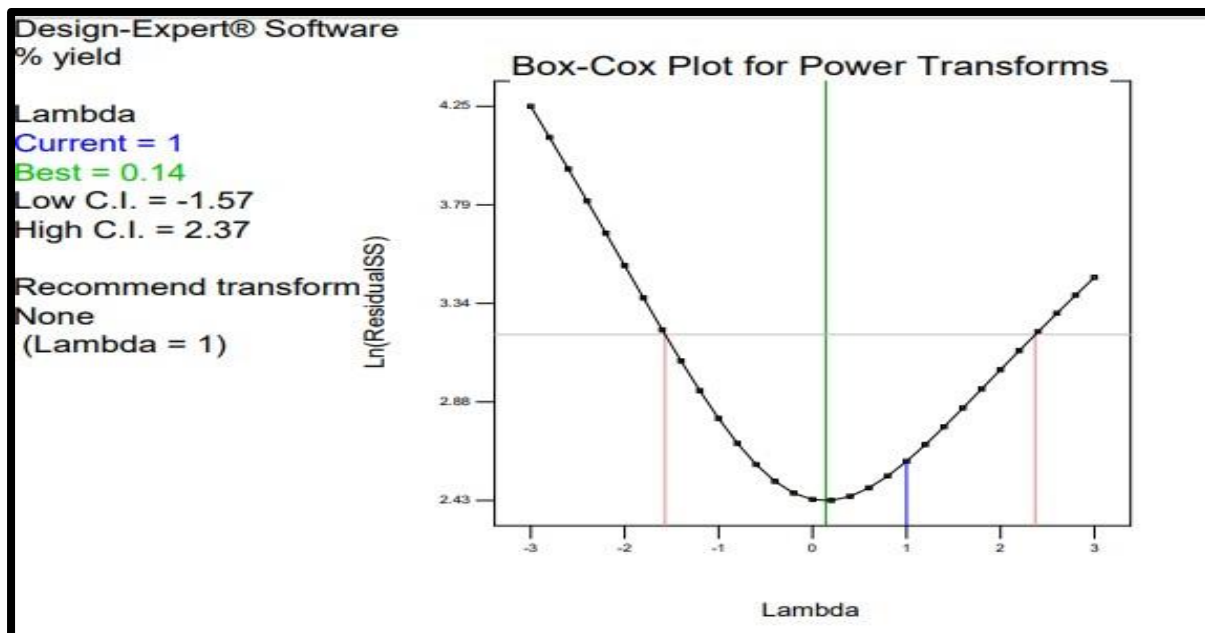

Figure 6.14 Box Cox plot for power transformation for %yield

6.4.2.3.2.2 Piepel's Plot

A steep slope for factor A (surfactant concentration) and curvature for factor B (silica source concentration) and factor C (stirring temperature) as shown in figure 6.15 proves that response was sensitive to the factors. The line for surfactant concentration shows sharp deviation from normal which suggests that it had a great impact on yield.
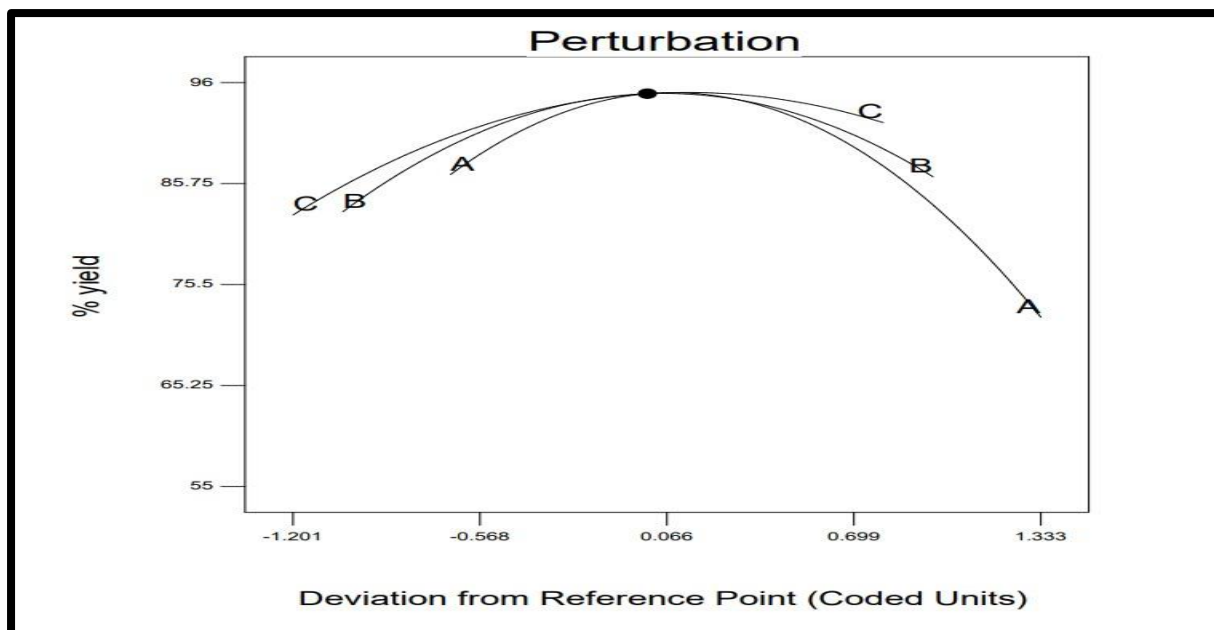
Figure 6.15 Piepel's plot

6.4.2.3.2.3 Response surface (3D) plots

The RED area in the Figure 6.16 shows the area of maximum %yield and BLUE zone represents the area with lowest %yield.
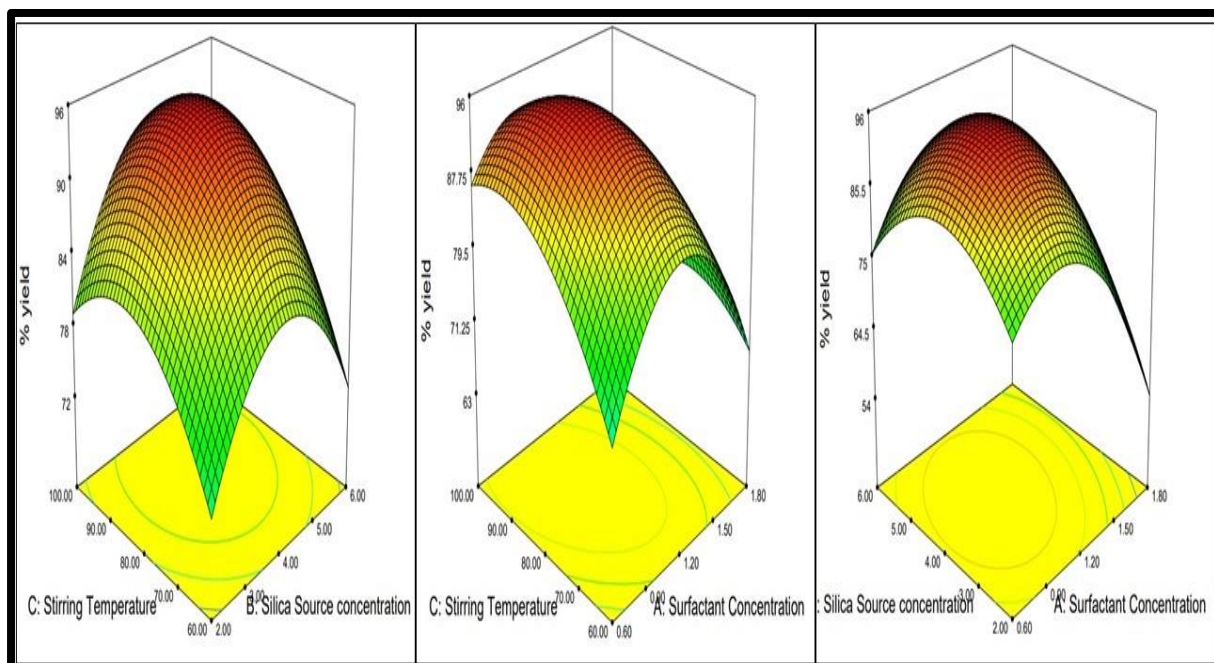
Figure 6.16 Response surface (3D) for yield

Two-factor 3D response surface plots for yield justifies the significant terms. A quadratic model was found to be best fit with the applied design and the higher cubic model was found

to be aliased. From the plots, it can be concluded that increasing the surfactant concentration and silica source concentration initially increases the yield but after a certain point, the yield decreases. This may be due to increased surfactant concentration leads to foaming that doesn't allow the formulation components to react and form nanoparticles that affects the overall yield.

6.4.2.3.2 Mathematical equation for %Yield

$$\% \text{ yield} = +93.67 - 6.37 \cdot A + 2.93 \cdot B + 2.99 \cdot C + 4.20 \cdot A \cdot B - 5.00 \cdot A \cdot C + 1.16 \cdot B \cdot C - 14.66 \cdot A^2 - 10.17 \cdot B^2 - 6.97 \cdot C^2 \text{ ----------- (6.3)}$$

6.6.3 Desirability plot for optimization

Desirability plot was generated using Design Expert 7.0. Parameters for the desirability batch are shown in Table 6.24.

Table 6.24 Variables for desirability plot and goals for response

Name	Goal	Lower Limit	Upper Limit
A: Surfactant Concentration (%)	In range	0.6	1.8
B: Silica Source Concentration (%)	In range	2	6
C: Stirring Temperature (°C)	In range	60	100
Quality Target			
Particle Size (nm)	Minimize	60	140
Surface Area (m^2/g)	Maximize	1080	1250
%Yield	Maximize	75	95
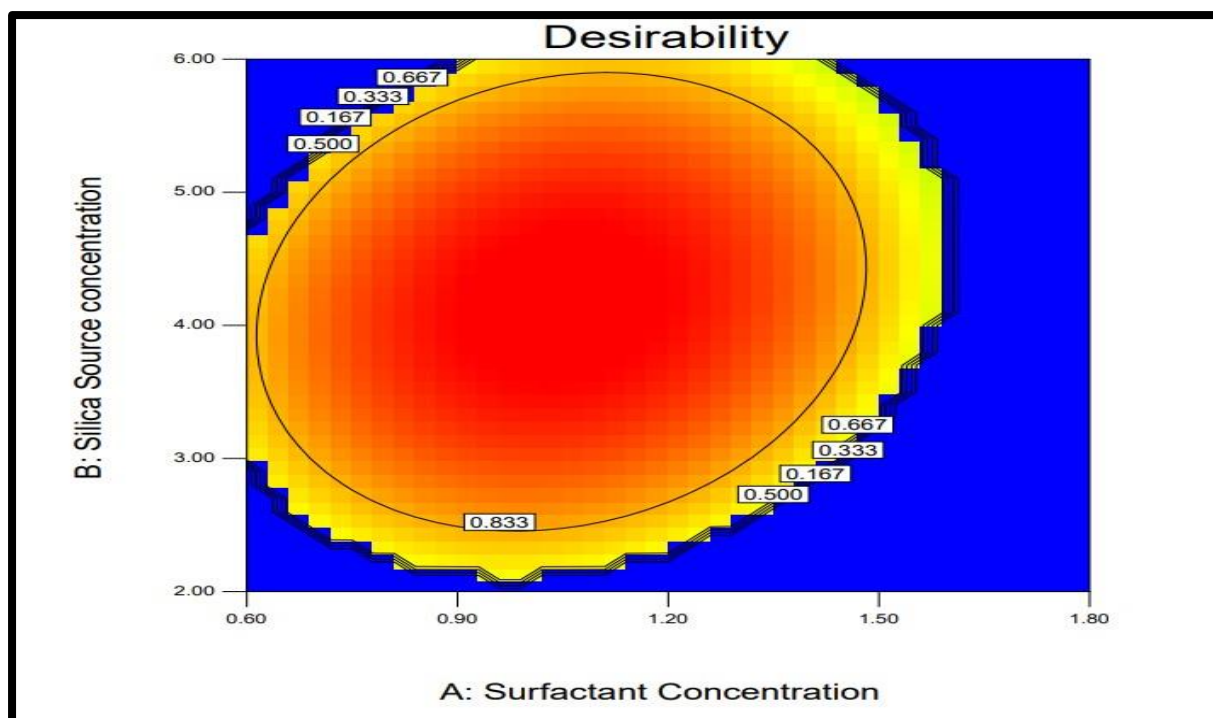
Figure 6.17 Desirability plot

6.4.4 Point prediction and confirmation

From the Box-Behnken design, three most desirable batches were selected for further optimization. Confirmation of the responses was done by carrying out the experiment using selected factor values in triplicate. (Shown in Table 6.26)

Table 6.25 Process parameters for optimized batch

Variables	Predicted Values	Actual values
A: Surfactant Concentration (%)	0.97	1.00
B: Silica Source Concentration (%)	3.98	4.00
C: Stirring Temperature (°C)	81.13	80.00

Table 6.26 Predicted vs Actual Experimental results

Batch No.	Parameters	Predicted values	Observed Values	%Error
1.	Particle Size (nm)	65.36	67.94 ± 2.31	3.94
2.	Surface Area (m²/g)	1241.59	1229.12 ± 23.65	1.64
3.	%Yield	94.18	95.86 ± 3.68	1.78

In this study, only drug free- MSNs were optimized using Box Behnken Design. The check point batches were prepared using the suggested concentrations for confirmation of reliability of design. The desirability value of optimized formulation was 0.833. The results of check point batches were evaluated and compared with predicted values. The results for particle size showed nearly 4 % error, this may be due to preparation of batch with rounding off the concentration suggested by the software, same goes with other results. The concentration of surfactant was increased by 0.03% which may have contributed to increase in particle size, as surfactant concentration showed maximum effect on particle size. Though, the limit for acceptance of error or bias is 5%, the design was found to be significant and unbiased.

6.5 Synthesis of amino functionalised nanoparticles (MSN – NH$_2$)

Synthesis of MSN – NH$_2$ was carried out using anhydrous toluene as a solvent. The typical procedure used for the synthesis of MSN – NH$_2$ was as follows:

MSN (1.0 g) was dispersed in 80 ml of anhydrous toluene, and then APTES was added into this dispersion in 3 different proportions (0.25 ml, 0.5 ml and 0.75ml). The reaction mixture was refluxed for 20h to yield the 3-aminopropyl-functionalized MSN (MSN-NH$_2$). The resulting mixture was centrifuged at 10,000 rpm, the supernatant was discarded and the pellet was washed several times with methanol. Finally, the product obtained was dried overnight under vacuum to obtain MSN-NH$_2$ as white precipitates (27).

The modification of MSNs with APTES was confirmed by performing various confirmatory tests such as (28):

- ✓ Zeta Potential
- ✓ FTIR – Spectroscopy
- ✓ Ninhydrin test

6.6 Synthesis of MSN – COOH

Carboxylation of MSNs was performed by Succinic anhydride (SA) as per previously reported procedure (29). In brief, 0.5 g of MSN – NH$_2$ were dispersed in 10 ml of anhydrous DMF and sonicated for 10 min. 10 ml of anhydrous DMF solution containing 3 g of SA was added and the reaction mixture was stirred at ambient temperature for 24h. Finally, the resulting powder was washed with methanol and water for several times and dried overnight at 60°C and denoted as MSN – COOH. The successful carboxylation of nanoparticles was confirmed by performing various confirmatory tests such as:

- ✓ Zeta Potential
- ✓ FT-IR Spectroscopy
- ✓ Ninhydrin test

6.7 Synthesis of folate conjugated MSN

The *N*-hydroxysuccinamide ester of folic acid (NHS-folate) was prepared through esterification of folic acid (1 mmol) with NHS (1 mmol) in dry dimethyl sulfoxide (DMSO, 0.4 mL) solution of EDC (2 mmol) and HOBT (1 mmol). The mixture was stirred under N_2 atmosphere for 30 minutes in an ice bath. Then, NHS-folate was added to the MSN-NH_2 suspension (MSN-NH_2 0.1 mg, DMSO 4 mL), and was stirred under N_2 atmosphere for 72 hours at room temperature. The mixture was washed with deionized water several times to produce MSN-FA (30).

PART B: Formulation of Drug loaded mesoporous silica nanoparticles (MSNs)

6.8.1 Formulation of Fulvestrant and Quercetin co-loaded MSNs Exemestane co loaded MSNs

The fulvestrant and quercetin co – loaded mesoporous silica nanoparticles were prepared by passive loading method. Briefly, 100 mg of MSN – NH_2 – COOH – FA was dispersed in 5 ml of methanol (31). Fulvestrant and Quercetin solution in concentration of 2.5 mg/ml and 5 mg/ml were prepared in 10 ml of methanol. Fulvestrant and quercetin solutions were mixed and sonicated for 10 minutes and stirred for 24 h. The resultant suspension was further centrifuged at 12000 rpm for 20 min to remove the unentrapped drug. The supernant for free drug was measured and encapsulation was calculated.

6.8.2 Formulation of Exemestane and Quercetin co-loaded MSNs

Briefly, 100 mg of MSN – NH_2 – COOH – FA was dispersed in 5 ml of methanol. Exemestane and Quercetin solution in concentration of 5 mg/ml for both, were prepared in 10 ml of methanol. Exemestane and Quercetin solutions were mixed and sonicated for 10 minutes and stirred for 24 h. The resultant suspension was further centrifuged at 12000 rpm for 20 min to remove the unentrapped drug. The supernant for free drug was measured and encapsulation was calculated.

6.9 CHARACTERIZATION

6.9.1 Encapsulation efficiency and Drug loading

The encapsulation efficiency and drug loading were evaluated by direct lysis method. Briefly, specified amount of drug loaded MSNs were suspended in 10 mL mixture of acetonitrile, methanol, and water (6.5:1.5:2) and sonicated for 3 minutes to extract the drug from MSN pores. The sample was further diluted and injected into HPLC system (Vanquish core, Thermofisher, MA, USA). The encapsulation and drug loading were calculated using following formula:

$$\% \ Encapsulation \ efficiency \ = \frac{Amount \ of \ drug \ entrapped}{Total \ amount \ of \ drug} \times 100 \qquad (\mathbf{6.4})$$

$$\% \ Drug \ Loading = \frac{Amount \ of \ drug \ in \ MSNs}{Total \ weight \ of \ MSNs} \times 100 \qquad (\mathbf{6.5})$$

6.9.2 Zeta Potential

The electrokinetic or zeta-potential is an important parameter of the electrical double layer and represents a characteristic of electrical properties of solid/liquid and liquid/gaseous interfaces. In contact with a polar medium (water), most particles show a definite surface charge as the consequence of ionization, ionic adsorption, and ionic dissolution. This surface charge influences the arrangement of neighbouring ions. Thus, it is related to the net electrostatic repulsion between the particles. Furthermore, it is also an important parameter to predict the biological interactions with blood protein, cell surface phagocytes and other molecules. To measure the zeta potential, the nanoparticles were suspended in doubled distilled water at concentration less than 5mg/ml and sonicated prior to measurement. The measurements were carried out in an automatic mode using Malvern Zetasizer Nano ZS (Malvern Panalytical), and the values were presented as an average value of 20 runs.

6.9.3 Ninhydrin Test

To determine primary amines content in the amine functionalized samples, ninhydrin colorimetric assay was performed as per the previously reported procedure with slight modifications: Briefly, small quantity (10 mg) of amine-functionalized MSN were dispersed in 0.2 mL of methanol and sonicated to form homogenous dispersion. The dispersion was allowed to react with 1 mL of ninhydrin solution (7.5 mg/mL) and placed in a boiling water bath for 15 minutes. The absorbance of the resulting solution was measured by UV-visible

spectrophotometer at 581 nm. The reaction of different known concentration of APTES with ninhydrin was applied for preparation of the calibration curve which was used for the quantification of amino groups (32).

6.9.4 Morphological characterization

Morphological characterization of the synthesized MSNs was performed using two different electron microscopy techniques: (1) Scanning electron microscopy (SEM), and (2) Transmission electron microscopy (TEM). The procedure for the same has been given in Chapter 3.

6.9.5 Surface area measurement by BET analysis

The surface area is one of the most important quantities for characterizing novel porous materials. The method for BET analysis has been given in Chapter 3.

6.9.6 In-vitro drug release study and drug release kinetics

The in vitro drug release studies were carried out as per the procedure described in Chapter 3, section 3.2.5.

6.9.7 Hemocompatibility Studies

For hemolysis assay, the red blood cells (RBCs) were isolated from chicken blood obtained from government approved slaughterhouse. Fresh blood was collected in dipotassium EDTA treated tubes and plasma was removed as supernatant by centrifugation at 3000 rpm for 10 min. The RBCs pellet was refined by successive rinsing with PBS buffer (pH 7.4). The suspension of RBC was diluted 10 times with PBS buffer (pH 7.4), and then 200 μL of RBCs suspension was added to 800 μL of free FLV and FLV formulations and for the free EXE and EXE formulations with different concentration (1, 20, 50, 100 μg/mL). For positive control, 200 μL of RBCs suspension was added to 800 μL Triton X100 (2% v/v), and for negative control, 200 μL of RBCs suspension was added to 800 μL of PBS buffer (pH 7.4). Afterwards, all the samples were incubated for 2 h in a shaker incubator. Finally, the samples were centrifuged at 10,000 rpm for 2 min, and the absorbance of supernatant (haemoglobin) was measured by UV-visible spectrophotometer at 398 nm (33). The haemolytic activity percentages of the different samples were calculated as follows:

$$\%Haemolysis = \frac{Abs\,(Sample) - Abs\,(Ctrl-)}{Abs\,(Ctrl+) - Abs\,(Ctrl-)} \tag{6}$$

6.10 RESULTS AND DISCUSSION

6.10.1 Physicochemical Characterization

Various physicochemical parameters of the optimized MCM – 41 types of MSNs, synthesized under the alkaline conditions, are shown in Table 6.27.

Table 6.27 Physicochemical characterization of MCM – 41 types of MSNs

Sr. No.	Physicochemical Parameters	Results
1	Nature	Solid Fine powder
2	Colour	White
3	Odour	None
4	Yield (%)	95.86 %
5	Density (g/ml)	0.21

6.10.2 Synthesis of MSN-NH$_2$ and MSN-NH$_2$-COOH

The success of amination and carboxylation over MSNs surface was confirmed by zeta potential and FTIR spectroscopic analysis. The changes in zeta potential on functionalization is given in Section 6.10.2. Figure 6.20 A and B compares the FTIR 0f non functionalized and amino functionalized MSNs whereas, Figure 6.20 C gives the FTIR spectra of COOH functionalized MSNs. The absorption signal shown by MSNs at 1094 cm^{-1} representing the stretching vibration of Si-O-Si was retained after amino functionalization also. An additional absorption peak near 1645 cm^{-1} and 2921 cm^{-1} was observed in case of MSN-NH$_2$ which was not present in non -functionalized MSN. This additional peak indicates the presence of -NH$_2$ bending and NH$_2$ stretching.
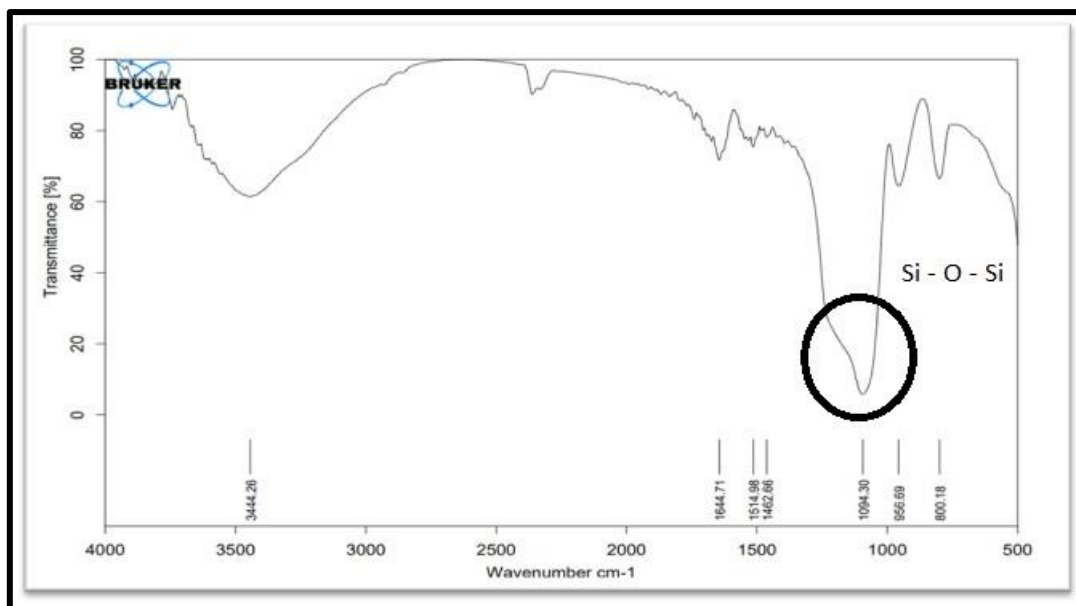
Figure 6.20A FTIR spectra of plain MSN
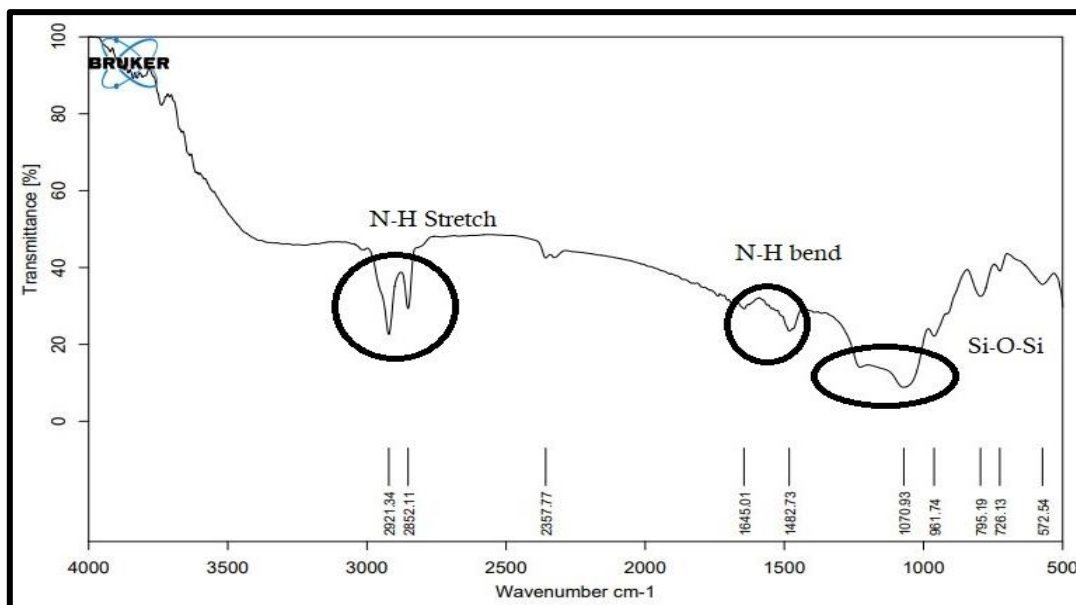
Figure 6.20B FTIR spectra for amino functionalized MSNs
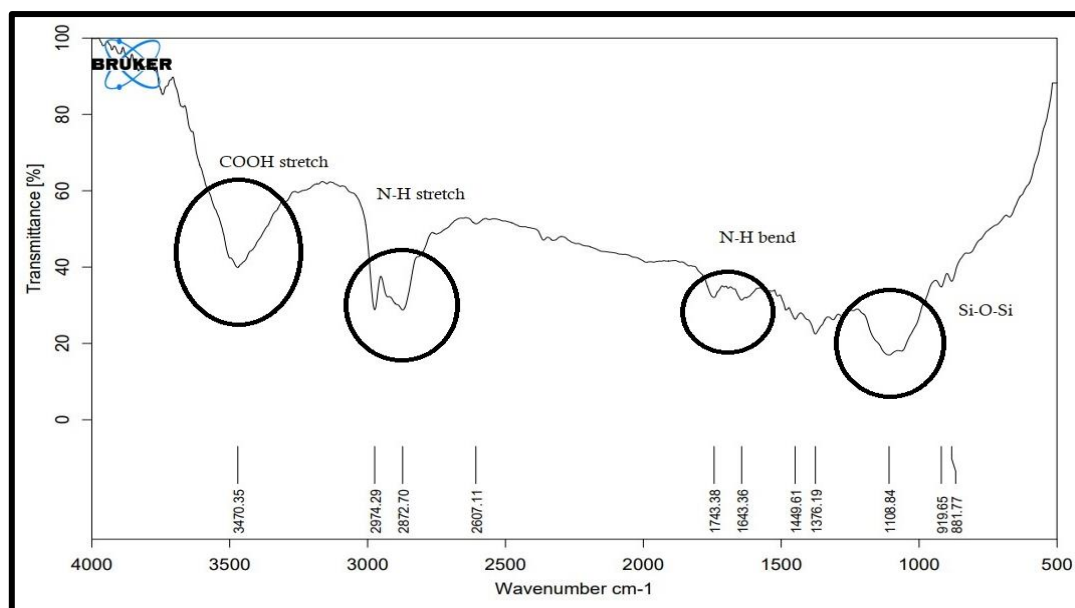
Figure 6.20C FTIR spectra of amino and COOH functionalized MSNs

6.10.3 Particle Size and Zeta Potential

The particle size and zeta potential of non-functionalized, functionalized, blank and drug loaded MSNs is shown in Table 6.28.

Table 6.28 Particle Size and Zeta potential of different MSN batches

Sr. No.	Sample	Particle Size	Zeta Potential
1.	MSNs	54.5 ± 1.52	-22.7 ± 1.54
2.	MSNs- NH_2	61.4 ± 2.13	$+26.5 \pm 2.31$
3.	MSNs-NH_2-COOH	69.7 ± 2.86	-11.5 ± 1.08
4.	MSN-NH_2-COOH-FA	86.2 ± 3.21	-17.1 ± 1.38
5.	FMSN	85.6 ± 3.62	-21.7 ± 2.14
6.	FQMSN	86.1 ± 4.19	-21.8 ± 2.52
7.	EMSN	86.5 ± 2.71	-21.6 ± 1.59
8.	EQMSN	86.5 ± 3.52	-22.4 ± 2.17

It was observed, as we functionalized the MSN core, there was a uniform and progressive increase in the particle size due to addition of functional groups on its surface. However, addition of the drug in the sample did not significantly increase the particle size, as the gets encapsulated in its pores and rather than on its surface. There was a significant difference in the zeta potentials of the sample. The zeta potential of blank MSNs was negative due to

presence of silica ions in the system. On functionalization with amines, they form ammonium ion which generates positive charge. Similarly, functionalization with carboxylic acid led to development of negative charge of the system taking the zeta potential of the system towards negative. Encapsulation of the drug in MSN further did not have any significant change in the zeta potential as the drug gets encapsulated in pores having negligible effect on the MSN properties.

6.10.4 Nitrogen adsorption/desorption study:

The specific surface areas were obtained by the Brunauer–Emmett–Teller (BET) method and pore size were achieved from the desorption graphs of the isotherms by BJH method (34). The Surface area for blank was found to be 1229.12 ± 23.65 m^2/g, pore size was found to be 16.9 ± 1.48 nm and pore volume was found to be 4.027 ± 0.65 cm^3/g.
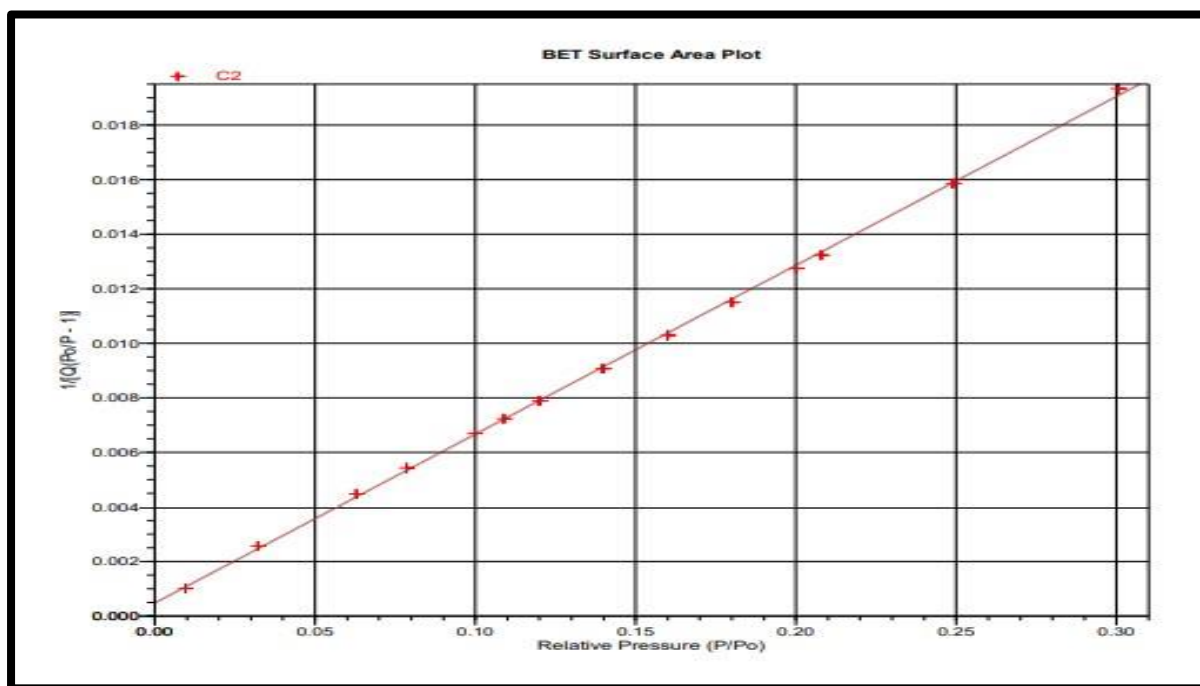
Figure 6.21 Linear Isotherm plot of MSNs

MSNs showed high pore diameter, pore volume, and surface area. On drug encapsulation, the surface area was found to reduce as it encapsulates into MSN core, leading to low space permeation of nitrogen which gave the low surface area results which are shown in Table 6.29.

Sr. No.	Sample	Surface area (m^2/g)	Pore size (nm)	Pore volume (cm^3/g)
1.	MSN-NH$_2$-COOH-FA	1229.12 ± 23.65	16.9 ± 1.48	4.027 ± 0.65

2.	QMSN	714.8 ± 14.21	8.3 ± 0.45	3.061 ± 0.38
3.	FMSN	561.2 ± 11.43	6.8 ± 0.36	2.213 ± 0.31
4.	FQMSN	319.6 ± 9.66	4.1 ± 0.19	1.762 ± 0.19
5.	EMSN	634.4 ± 17.24	7.4 ± 0.31	2.401 ± 0.23
6.	EQMSN	445.1 ± 12.28	5.5 ± 0.24	1.951 ± 0.18

The surface area reduced as the drug was encapsulated in the MSN cores, the reduction in surface area was the result of molecular weight of drug encapsulated. As the molecular weight increases the more surface area was covered leading to reduction in overall surface area of blank MSNs.

6.10.5 Morphological Characterization:

Morphological Characterization of synthesized nanoparticles was performed using two different techniques: TEM and FEG-SEM.

6.10.5.1 TEM imaging:

TEM images were captured with a view to analyze the physical morphology as well as pore channel structure of the synthesized MSNs. As shown in Figure 6.22, MSNs were nearly spherical to ellipsoidal in shape. A highly ordered mesoporous network with a hexagonal array with honeybee network could be clearly seen in the MSN structure. The particle size of 54.06 nm on TEM scale.
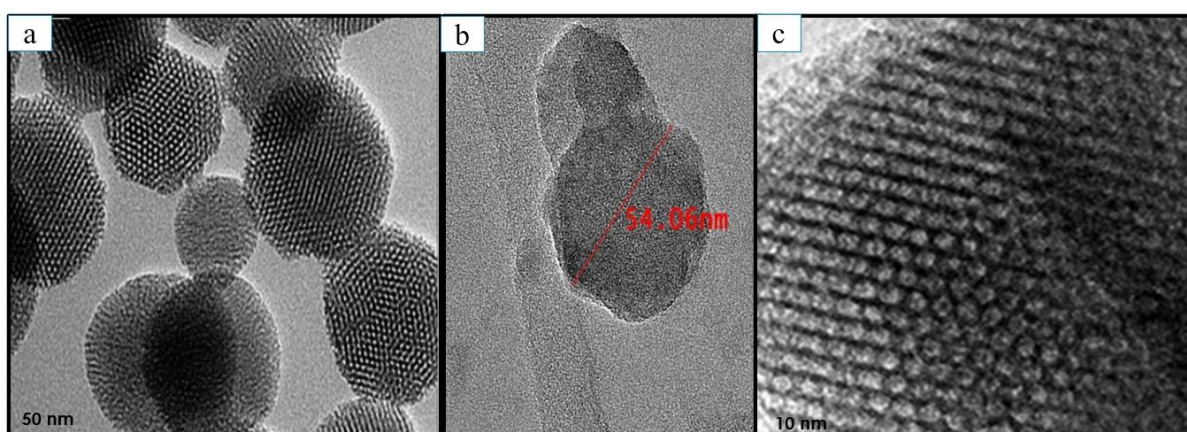
Figure 6.22 TEM analysis of MSNs (a) MSN bulk (b) Single MSN (c) Hexagonal array

6.10.5.2 FEG – SEM imaging

The morphology of MSNs was further confirmed by FEG – SEM imaging. The particles were found to be having uniform spherical morphology with average particle size of 84 ± 3 nm.
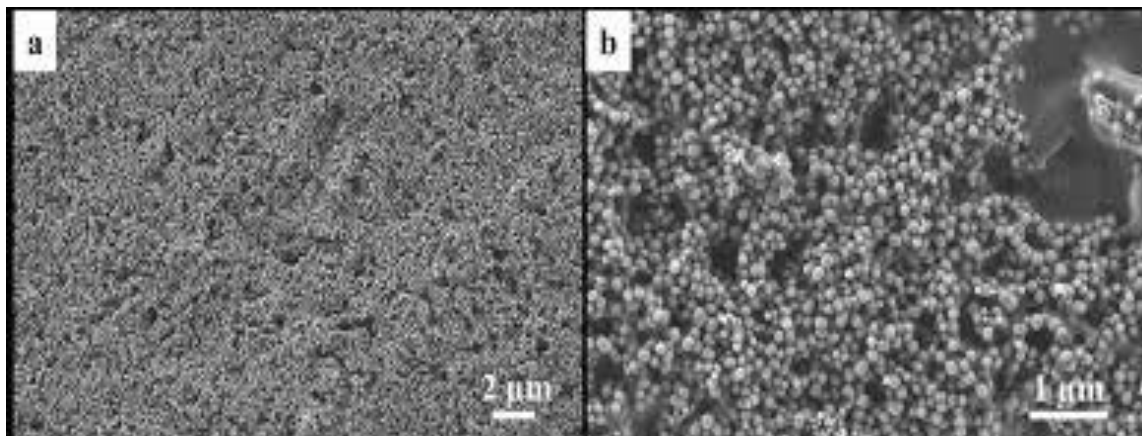
Figure 6.23 FEG – SEM images MSN (a) 2 µm scale, 10000x (b) 1 µm scale, 20000x

6.10.6 In-vitro drug release study and drug release kinetics (Fulvestrant)

Fulvestrant loaded MSNs have followed the sustained release kinetics (Figure 6.24a). From the three pH conditions, the highest release curve was observed in pH 5.5, which suggested maximum release of the drug in cancer cells. Release of the fulvestrant from the MSNs in the different media was observed to be in decreasing order of pH 5.5 > pH 6.6 > pH 7.4, which indicates the least drug release in plasma and blood. The sustained release of fulvestrant was achieved owing to the presence of drug in MSN pores (35). The release of fulvestrant suspension was found to be completed within 24 hours, indicating the need for dose administration frequently (Figure 6.24b). There was no significant difference in the drug release pattern in different pH conditions.
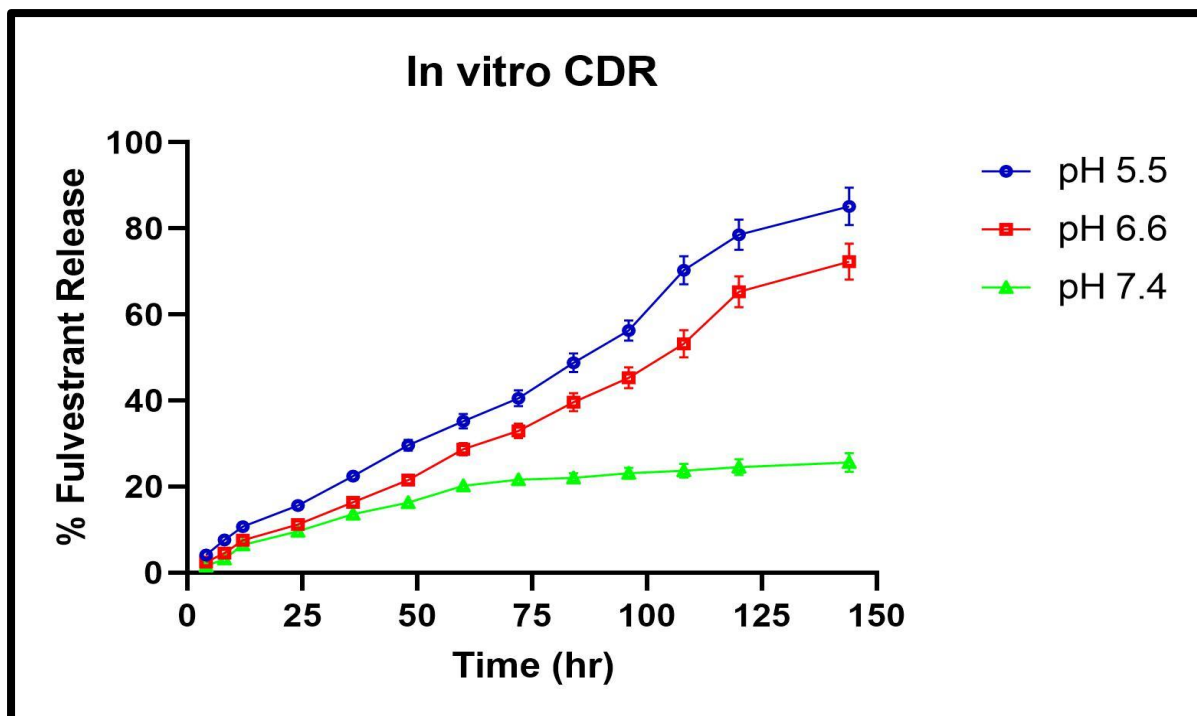
Figure 6.24 (a) Fulvestrant MSN release pattern in different release media
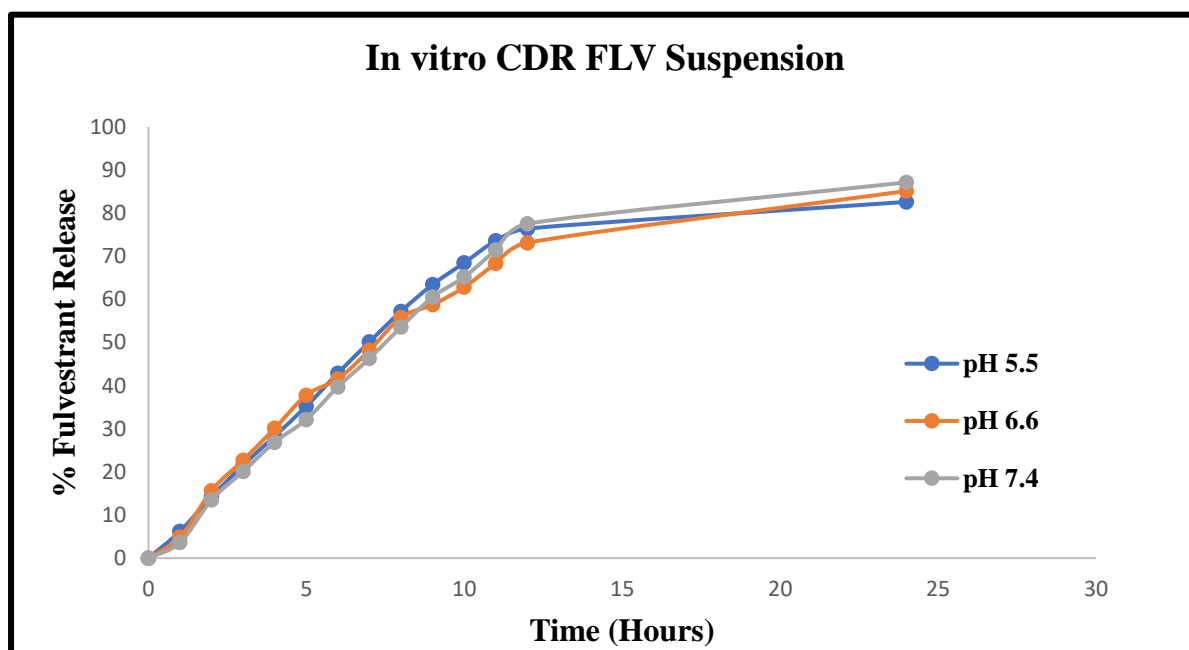
**Figure 6.24 (b) In vitro drug release of fulvestrant suspension**
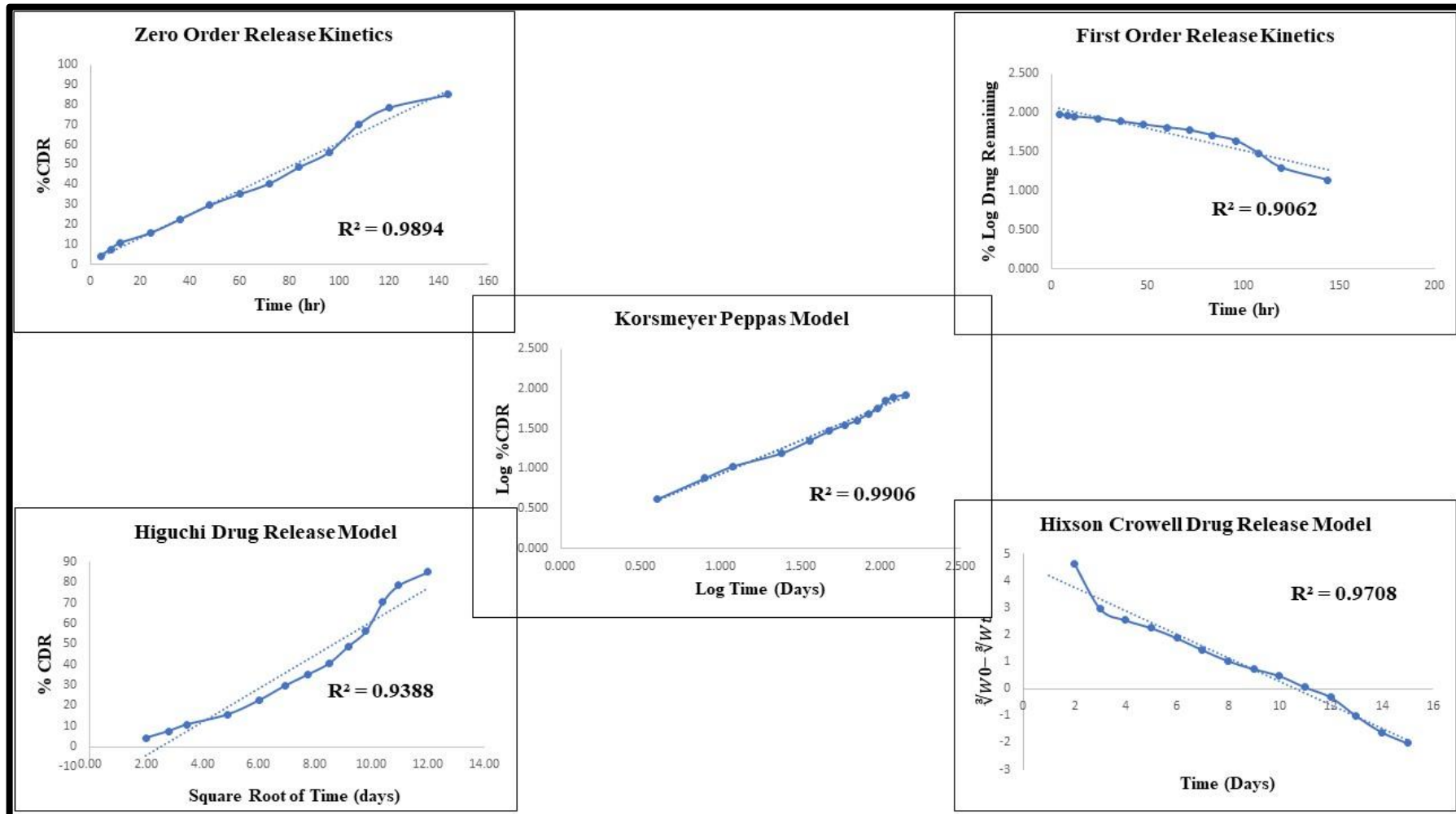
Figure 6.25 In Vitro Drug release Model for Fulvestrant

From the kinetic model fitting analysis, it was concluded that for the fulvestrant loaded MSNs, the best fit was Korsmeyer Peppas model (Figure 6.25) with the R^2 value of 0.9906, with the n value of 0.835, which is consistent with the drug release by anomalous transport or non-Fickian diffusion that involves two phenomena: drug diffusion and relaxation of the polymer matrix. The comparison of models is shown in Table 6.29.

Table 6.29 Drug release kinetics Fulvestrant MSNs

Model	Regression Coefficient
Zero Order	0.9894
First Order	0.9062
Higuchi	0.9388
Korsmeyer Peppas	0.9906
Hixson Crowell	0.9708

6.10.7 In-vitro drug release study and drug release kinetics (Exemestane)

Exemestane loaded MSNs have followed the sustained release kinetics (Figure 6.26). From the three pH condition, the highest release was found in pH 5.5, which suggested maximum release of drug in cancer cells. Release of exemestane from the MSNs in the different media was observed to be in decreasing order of pH 5.5 > pH 6.6 > pH 7.4, which indicates least drug release in plasma and blood.
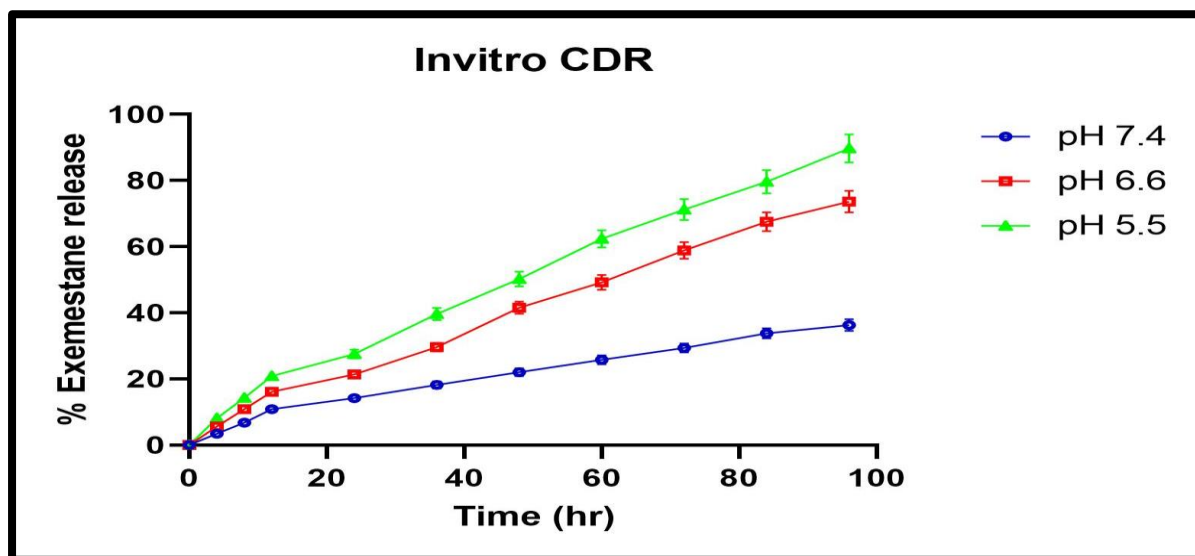

**Figure 6.26 Exemestane MSN release pattern in different release media**
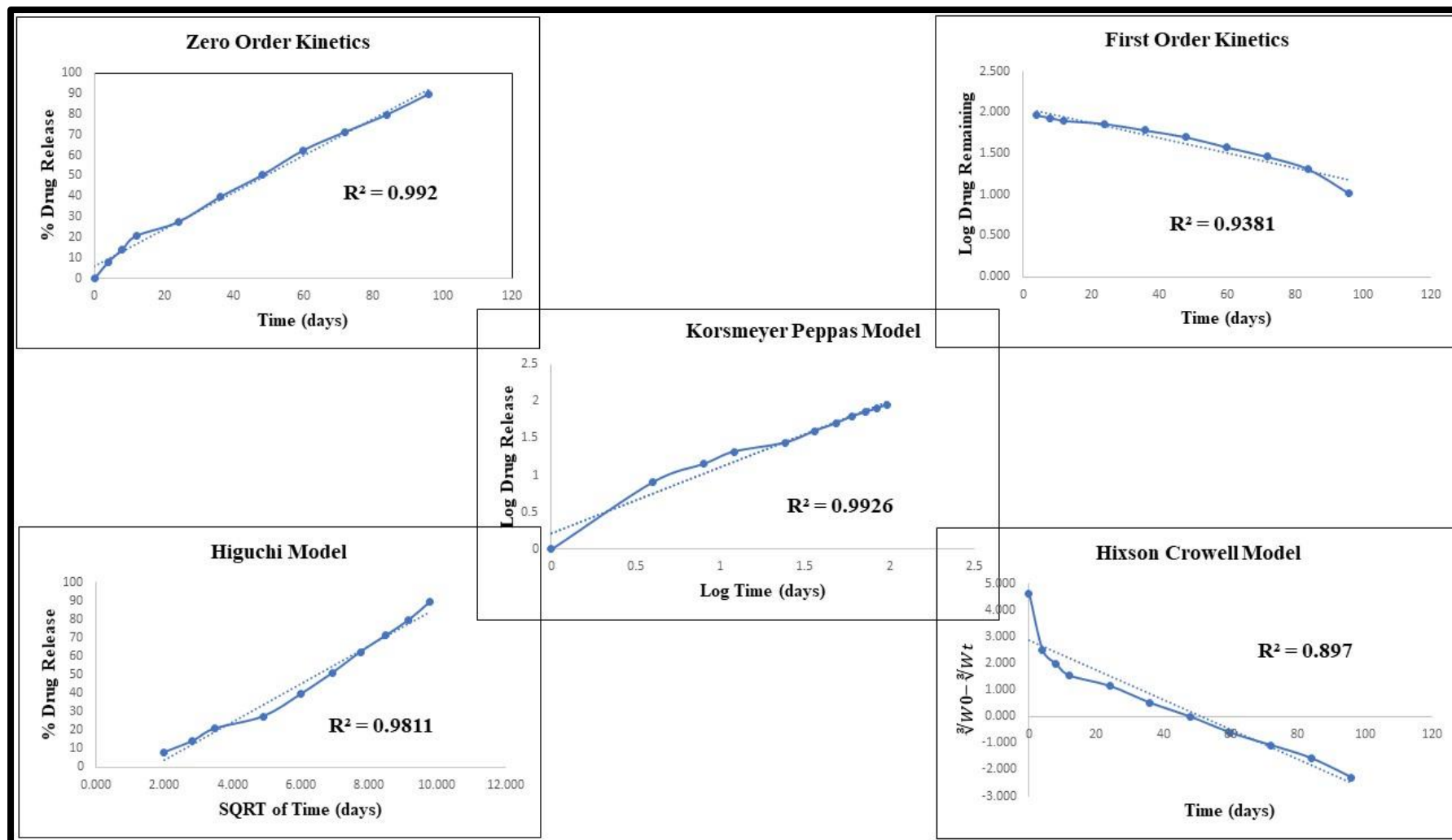
Figure 6.27 In Vitro Drug release Model for Exemestane

From the kinetic model fitting analysis, it was concluded that for exemestane and quercetin co-loaded MSNs, the best fit model was Korsmeyer Peppas model (Figure 6.27) with the R^2 value of 0.9926, with the n value of 0.892, which is consistent with the drug release by anomalous transport or non-Fickian diffusion that involves two phenomena: drug diffusion and relaxation of the polymer matrix. The comparison of model is shown in Table 6.30.

Table 6.30 Drug release kinetics Exemestane MSNs

Model	Regression Coefficient
Zero Order	0.9920
First Order	0.9381
Higuchi	0.9811
Korsmeyer Peppas	0.9926
Hixson Crowell	0.8970

6.10.8 In-vitro drug release study (Quercetin)

Quercetin suspension showed pH independent drug release with complete release within 13h. It followed zero order release kinetics and portrayed controlled release pattern due to low aqueous solubility of quercetin.
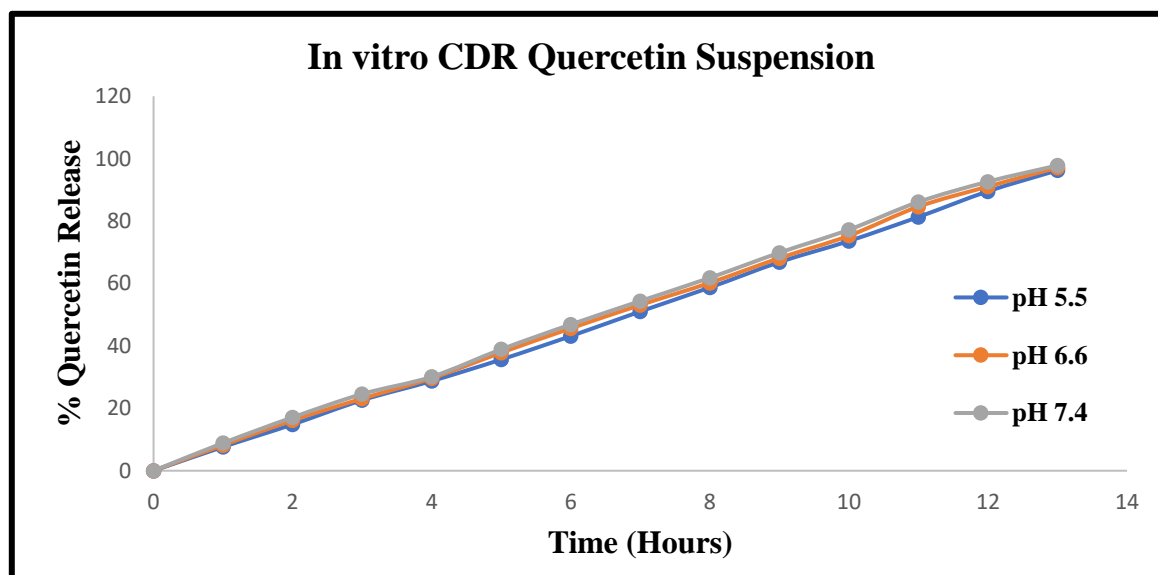

**Figure 6.28 Quercetin drug release from suspension**
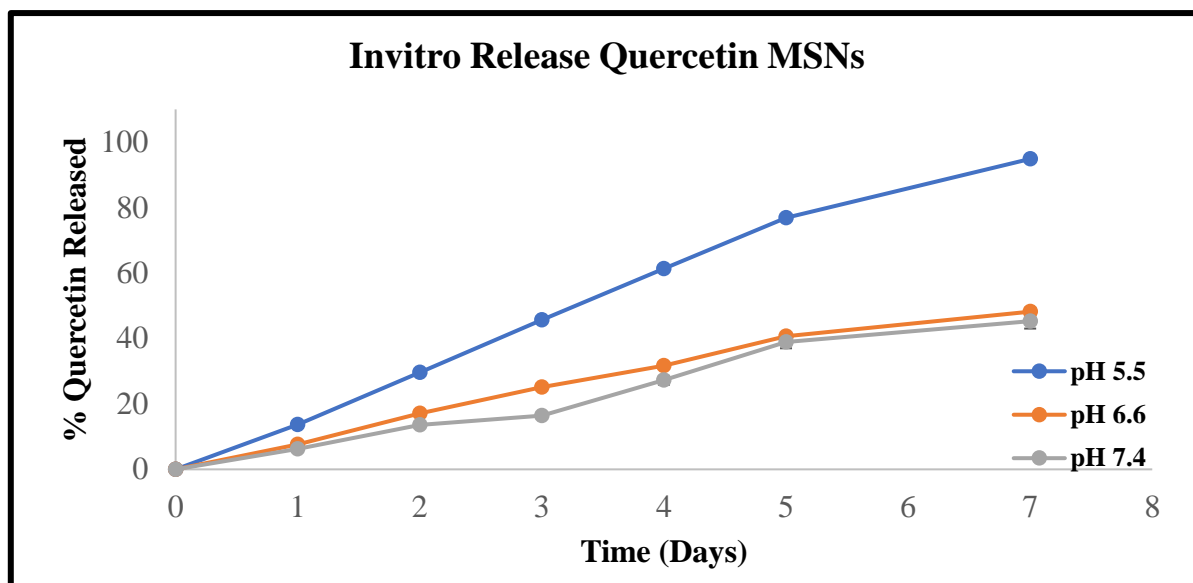
Figure 6.29 Quercetin MSN release pattern from different media

Quercetin loaded MSNs followed the sustained release kinetics (Figure 6.29). From the three pH condition, the highest release was found in pH 5.5, which suggested maximum release of drug in cancer cells. Release of quercetin from the MSNs in the different media was observed to be in decreasing order of pH 5.5 > pH 6.6 > pH 7.4, which indicates least drug release in plasma and blood. The drug release kinetics followed Korsmeyer Peppas release kinetic model.

6.10.9 Hemocompatibility Studies

Hemocompatibility of functionalized drug loaded nanoparticles was confirmed by performing the in vitro hemolysis study and the effect of plain drug and various drug formulations was checked on the erythrocytes.
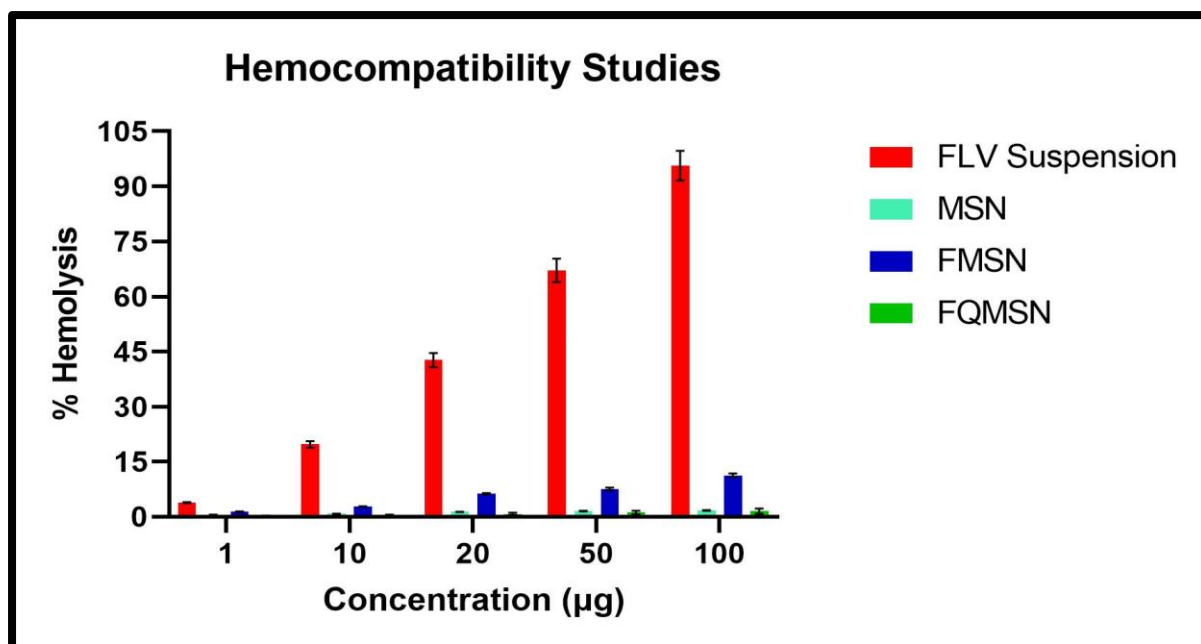
Figure 6.30 Hemocompatibility study for Fulvestrant MSN

As seen in the figure 6.30, as the concentration of FLV increased, the percent hemolysis increased. At higher concentration, plain FLV caused 96% hemolysis. The incorporation of FLV into MSN showed considerable reduction in hemolysis and the FQMSNs loaded with quercetin and fulvestrant showed minimum hemolysis. This must be due to fast release of FLV and its interaction with erythrocytes. As the drug was encapsulated within MSN core, the drug erythrocyte interaction was very less, significantly reducing hemolysis and increasing biocompatibility of FQMSN.
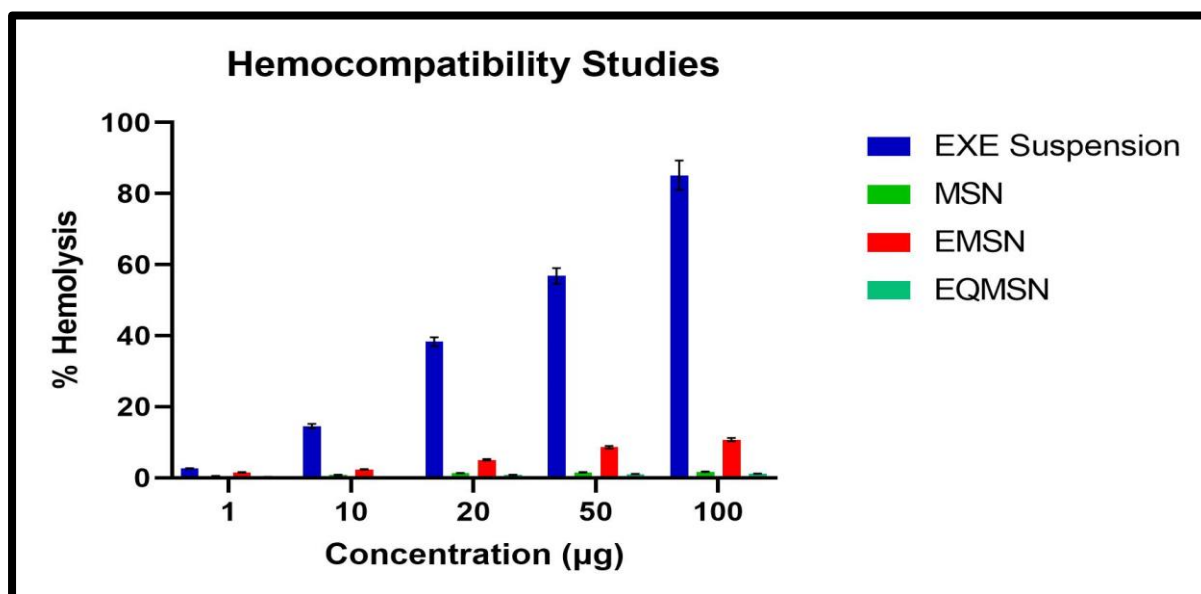

Figure 6.31 Hemocompatibility study for Exemestane MSN

As seen in the figure 6.31, as the concentration of EXE increased, the percent hemolysis increased. At higher concentration, plain EXE caused 85% hemolysis. The incorporation of EXE into MSN showed considerable reduction in hemolysis. The MSNs loaded with quercetin and exemestane and having folate conjugation showed minimum hemolysis.

References

1. Parra-Nieto J, del Cid MAG, de Cárcer IA, Baeza A. Inorganic Porous Nanoparticles for Drug Delivery in Antitumoral Therapy. Biotechnology Journal. 2021;16(2):2000150.
2. Colilla M, Vallet-Regí M. Targeted Stimuli-Responsive Mesoporous Silica Nanoparticles for Bacterial Infection Treatment. International Journal of Molecular Sciences. 2020;21(22).
3. Fernandes RS, Raimundo Jr IM, Pimentel MF. Revising the synthesis of Stöber silica nanoparticles: A multivariate assessment study on the effects of reaction parameters on the particle size. Colloids and Surfaces A: Physicochemical and Engineering Aspects. 2019;577:1-7.
4. Kim T-W, Chung P-W, Lin VSY. Facile Synthesis of Monodisperse Spherical MCM-48 Mesoporous Silica Nanoparticles with Controlled Particle Size. Chemistry of Materials. 2010;22(17):5093-104.
5. Li H, Chen Y, Liu S, Liu Q. Enhancement of hydrothermal synthesis of FDU-12-derived nickel phyllosilicate using double accelerators of ammonium fluoride and urea for CO2 methanation. Journal of CO2 Utilization. 2021;52:101677.
6. Colmenares MG, Simon U, Schmidt F, Dey S, Schmidt J, Thomas A, et al. Tailoring of ordered mesoporous silica COK-12: Room temperature synthesis of mesocellular foam and multilamellar vesicles. Microporous and Mesoporous Materials. 2018;267:142-9.
7. Lv X, Zhang L, Xing F, Lin H. Controlled synthesis of monodispersed mesoporous silica nanoparticles: Particle size tuning and formation mechanism investigation. Microporous and Mesoporous Materials. 2016;225:238-44.
8. Mohamad DF, Osman NS, Nazri MKHM, Mazlan AA, Hanafi MF, Esa YAM, et al. Synthesis of Mesoporous Silica Nanoparticle from Banana Peel Ash for Removal of Phenol and Methyl Orange in Aqueous Solution. Materials Today: Proceedings. 2019;19:1119-25.
9. Vazquez NI, Gonzalez Z, Ferrari B, Castro Y. Synthesis of mesoporous silica nanoparticles by sol–gel as nanocontainer for future drug delivery applications. Boletín de la Sociedad Española de Cerámica y Vidrio. 2017;56(3):139-45.
10. Sun B, Chai J, Chai Z, Zhang X, Cui X, Lu J. A surfactant-free microemulsion consisting of water, ethanol, and dichloromethane and its template effect for silica synthesis. Journal of colloid and interface science. 2018;526:9-17.
11. Khoeini M, Najafi A, Rastegar H, Amani M. Improvement of hollow mesoporous silica nanoparticles synthesis by hard-templating method via CTAB surfactant. Ceramics International. 2019;45(10):12700-7.
12. Asgari M, Soleymani M, Miri T, Barati A. A robust method for fabrication of monodisperse magnetic mesoporous silica nanoparticles with core-shell structure as anticancer drug carriers. Journal of Molecular Liquids. 2019;292:111367.
13. Chen QGYGHHS-PEoEoAMSFbISMSM. Nanomaterials [Internet]. 2018; 8(6).
14. Kankala RK, Han YH, Na J, Lee CH, Sun Z, Wang SB, et al. Nanoarchitectured structure and surface biofunctionality of mesoporous silica nanoparticles. Advanced materials. 2020;32(23):1907035.

15.   Wang X, Li C, Fan N, Li J, Zhang H, Shang L, et al. Amino functionalized chiral mesoporous silica nanoparticles for improved loading and release of poorly water-soluble drug. Asian journal of pharmaceutical sciences. 2019;14(4):405-12.

16.   Nik AB, Zare H, Razavi S, Mohammadi H, Ahmadi PT, Yazdani N, et al. Smart drug delivery: Capping strategies for mesoporous silica nanoparticles. Microporous and Mesoporous Materials. 2020;299:110115.

17.   Pal N, Lee J-H, Cho E-B. Recent trends in morphology-controlled synthesis and application of mesoporous silica nanoparticles. Nanomaterials. 2020;10(11):2122.

18.   Mohamed Isa ED, Abdul Rahman MB, Ahmad H. Monodispersed mesoporous silica nanospheres based on pyridinium ionic liquids. Journal of Porous Materials. 2018;25(5):1439-46.

19.   Travaglini L, Picchetti P, Del Giudice A, Galantini L, De Cola L. Tuning and controlling the shape of mesoporous silica particles with CTAB/sodium deoxycholate catanionic mixtures. Microporous and Mesoporous Materials. 2019;279:423-31.

20.   Abduraimova A, Molkenova A, Duisembekova A, Mulikova T, Kanayeva D, Atabaev TS. Cetyltrimethylammonium bromide (CTAB)-loaded SiO_2–Ag mesoporous nanocomposite as an efficient antibacterial agent. Nanomaterials. 2021;11(2):477.

21.   Hwang J, Lee JH, Chun J. Facile approach for the synthesis of spherical mesoporous silica nanoparticles from sodium silicate. Materials Letters. 2021;283:128765.

22.   Bhavsar D, Patel V, Sawant K. Systematic investigation of in vitro and in vivo safety, toxicity and degradation of mesoporous silica nanoparticles synthesized using commercial sodium silicate. Microporous and Mesoporous Materials. 2019;284:343-52.

23.   Chen Z, Han S, Shi M, Liu G, Chen Z, Chang J, et al. Immunomodulatory effects of mesoporous silica nanoparticles on osteogenesis: from nanoimmunotoxicity to nanoimmunotherapy. Applied Materials Today. 2018;10:184-93.

24.   Kachbouri S, Mnasri N, Elaloui E, Moussaoui Y. Tuning particle morphology of mesoporous silica nanoparticles for adsorption of dyes from aqueous solution. Journal of Saudi Chemical Society. 2018;22(4):405-15.

25.   Guo Z, Wu L, Wang Y, Zhu Y, Wan G, Li R, et al. Design of dendritic large-pore mesoporous silica nanoparticles with controlled structure and formation mechanism in dual-templating strategy. ACS applied materials & interfaces. 2020;12(16):18823-32.

26.   Harun SN, Ahmad H, Lim HN, Chia SL, Gill MR. Synthesis and optimization of mesoporous silica nanoparticles for ruthenium polypyridyl drug delivery. Pharmaceutics. 2021;13(2):150.

27.   Mehmood Y, Khan IU, Shahzad Y, Khan RU, Khalid SH, Yousaf AM, et al. Amino-decorated mesoporous silica nanoparticles for controlled sofosbuvir delivery. European journal of pharmaceutical sciences. 2020;143:105184.

28.   Nairi V, Magnolia S, Piludu M, Nieddu M, Caria CA, Sogos V, et al. Mesoporous silica nanoparticles functionalized with hyaluronic acid. Effect of the biopolymer chain length on cell internalization. Colloids and Surfaces B: Biointerfaces. 2018;168:50-9.

29.   Li Y, Wang S, Song FX, Zhang L, Yang W, Wang HX, et al. A pH-sensitive drug delivery system based on folic acid-targeted HBP-modified mesoporous silica nanoparticles for cancer therapy. Colloids and Surfaces A: Physicochemical and Engineering Aspects. 2020;590:124470.

30.   Tonbul H, Sahin A, Tavukcuoglu E, Ultav G, Akbas S, Aktas Y, et al. Folic acid decoration of mesoporous silica nanoparticles to increase cellular uptake and cytotoxic activity of doxorubicin in human breast cancer cells. Journal of Drug Delivery Science and Technology. 2021;63:102535.

31.   Liu M, Fu M, Yang X, Jia G, Shi X, Ji J, et al. Paclitaxel and quercetin co-loaded functional mesoporous silica nanoparticles overcoming multidrug resistance in breast cancer. Colloids and Surfaces B: Biointerfaces. 2020;196:111284.

32.   Della Rosa G, Di Corato R, Carpi S, Polini B, Taurino A, Tedeschi L, et al. Tailoring of silica-based nanoporous pod by spermidine multi-activity. Scientific Reports. 2020;10(1):21142.

33.   Lin X, Wu W, Fu J, Yang Y, Guo B, Yu C, et al. Asymmetric Silica Nanoparticles with Tailored Spiky Coverage Derived from Silica–Polymer Cooperative Assembly for Enhanced Hemocompatibility and Gene Delivery. ACS Applied Materials & Interfaces. 2021;13(43):50695-704.

34.   Li X, Xie C, Xia H, Wang Z. pH and ultrasound dual-responsive polydopamine-coated mesoporous silica nanoparticles for controlled drug delivery. Langmuir. 2018;34(34):9974-81.

35.   LaBauve AE, Rinker TE, Noureddine A, Serda RE, Howe JY, Sherman MB, et al. Lipid-coated mesoporous silica nanoparticles for the delivery of the ML336 antiviral to inhibit encephalitic alphavirus infection. Scientific reports. 2018;8(1):1-13.